

# Bifurcation analysis of multiple limit cycles created in boundary equilibrium bifurcations in hybrid systems\*

Hong Tang <sup>†</sup>    Alan Champneys <sup>‡</sup>    David J.W. Simpson <sup>§</sup>

December 11, 2024

## Abstract

A boundary equilibrium bifurcation (BEB) in a hybrid dynamical system occurs when a regular equilibrium collides with a switching surface in phase space. This causes a transition to a pseudo-equilibrium embedded within the switching surface, but limit cycles (LCs) and other invariant sets can also be created and the nature of these is not well understood for systems with more than two dimensions. This work treats two codimension-two scenarios in hybrid systems of any number of dimensions, where the number of small-amplitude limit cycles bifurcating from a BEB changes. The first scenario involves a limit cycle (LC) with a Floquet multiplier 1 and for nearby parameter values the BEB creates a pair of limit cycles. The second scenario involves a limit cycle with a Floquet multiplier  $-1$  and for nearby parameter values the BEB creates a period-doubled solution. Both scenarios are unfolded in a general setting, showing that typical two-parameter bifurcation diagrams have a curve of saddle-node or period-doubling bifurcations emanating transversally from a curve of BEBs at the codimension-two point. The results are illustrated

---

\*Manuscript draft

**Funding:** Hong Tang was funded by the China Scholarship Council; David Simpson was supported by Marsden Fund contract MAU2209 managed by Royal Society Te Apārangi.

<sup>†</sup>Department of Engineering Mathematics, University of Bristol, Bristol BS8 1TR, UK (hong.tang@bristol.ac.uk).

<sup>‡</sup>Department of Engineering Mathematics, University of Bristol, Bristol BS8 1TR, UK (A.R.Champneys@bristol.ac.uk).

<sup>§</sup>School of Mathematical and Computational Sciences, Massey University, Palmerston North, 4410, New Zealand (D.J.W.Simpson@massey.ac.nz).

with three-dimensional examples and an eight-dimensional airfoil model. Detailed computational results show excellent agreement to the unfolding theory and reveal further interesting dynamical features that remain to be explored.

**Keywords:** Impact, periodic orbits, saddle-node, period doubling, boundary equilibrium bifurcation, hybrid system

## 1 Introduction

To understand the behaviour of a dynamical system, it is helpful to identify *bifurcations* where the dynamics changes in a fundamental way. There is a well established and extensive theory for bifurcations that has proved to be highly successful at explaining the dynamical behaviour of diverse systems in science, engineering, and medicine (and beyond), in part because much of the theory places no restriction on the system dimension, i.e. the number of variables. This occurs when the pertinent dynamics belongs to a centre manifold that is one or two dimensional for most common bifurcations [28].

But this dimension reduction requires that the equations of motion are smooth. For piecewise-smooth ODEs (ordinary differential equations) and hybrid systems, many basic bifurcations do not involve a centre manifold. The phase spaces of such systems have codimension-one switching surfaces where, in the case of piecewise-smooth systems, the functional form of the ODEs changes [9, 11, 24]. Hybrid systems have reset laws (maps) that specify an instantaneous change to the state of system whenever it reaches a switching surface [18, 32]. These systems are used to model a wide variety of mechanical and control systems, particularly vibro-impacting systems with hard unilateral constraints and systems that combine digital and analog elements [5, 23, 42].

The simplest type of bifurcation unique to piecewise-smooth and hybrid systems is a *boundary equilibrium bifurcation* (BEB) whereby a regular equilibrium (zero of some smooth component of the ODEs) collides with a switching surface. As shown by di Bernardo *et al.* [3], if we look only at equilibria, there are two cases for the local dynamics occurring as we cross the BEB. Either the regular equilibrium is replaced by another equilibrium (*persistence*), or it collides and annihilates with a coexisting equilibrium (*nonsmooth fold*). For hybrid and Filippov systems the second equilibrium is a *pseudo-equilibrium* on the switching surface.

But BEBs readily generate other dynamics. For two-dimensional systems this is well understood; we refer to [14, 38] for continuous, non-differentiable ODEs, [15, 22, 27] for Filippov systems, and [3, 36] for hybrid systems. However, the dynamical

complexity increases with dimension [16] and already in three dimensions BEBs can create chaotic attractors regardless of whether the system is continuous [35], Filippov [6, 17, 31, 33], or hybrid [3].

Recent work of two of the authors [39] revealed a BEB with unusual characteristics in an eight-dimensional hybrid system modelling the motion of an airfoil. The system has a stable regular equilibrium corresponding to the airfoil in a fixed position. As the air velocity (a model parameter) is increased, the equilibrium undergoes a BEB whereby the airfoil flap hits a clamped stop. This bifurcation is of persistence type, leading to a stable pseudo-equilibrium where the flap is in contact with the stop. But the BEB also creates a stable limit cycle, and this is particularly interesting because the system then has multiple attractors and because such a transition is not possible for BEBs in two dimensions.

In this paper, to understand how such a BEB can arise we consider curves of BEBs in two-dimensional parameter space. Qualitative changes to the dynamics associated with the BEB occur at codimension-two points, such as where the regular equilibrium is non-hyperbolic. It is known that if the equilibrium has a zero eigenvalue then generically a curve of saddle-node bifurcation emanates from the curve of BEBs with a quadratic tangency, while if it has a pair of purely imaginary eigenvalues then generically a curve of Hopf bifurcations emanates transversally from the curve of BEBs [4, 19, 34, 37]. But in the airfoil model it is the limit cycle that is non-hyperbolic at a nearby codimension-two point. Such codimension-two BEBs do not appear to have been studied before, possibly being overlooked because they require at least three dimensions to occur generically.

Specially, we unfold two codimension-two scenarios where a BEB creates a non-hyperbolic limit cycle. We show that if the limit cycle has a Floquet multiplier of 1 then in two-dimensional parameter space a curve of saddle-node bifurcations (of limit cycles) emanates transversely from a curve of BEBs. On one side of the codimension-two point, the BEB creates two limit cycles, one of which can be stable and coexisting with a stable pseudo-equilibrium as observed in the airfoil model. We stress that the saddle-node and BEB curves meet transversally, which is different to previously reported cases where the saddle-node bifurcations are of equilibria [7, 37]. We also show that if the limit cycle has a Floquet multiplier of  $-1$ , then a curve of period-doubling bifurcations emanates transversely from the curve of BEBs. These unfoldings apply to impacting hybrid systems of three or more dimensions.

The remainder of this paper is organized as follows. Section 2 introduces general notation for impacting systems and BEBs, then Section 3 presents the main results proved using blow-up and centre-manifold techniques. Section 4 illustrates the results with three-dimensional examples and the airfoil model, then Section 5 draws

conclusions and suggests avenues for future work.

## 2 Impacting hybrid systems

Many vibro-impacting mechanical systems are well-modelled by treating objects as rigid and impact events as instantaneous. With this viewpoint, impacts bring about a discontinuous change to the velocity of objects. This leads to mathematical models that are hybrid systems, combining ODEs for the smooth evolution in open intervals of time with reset laws for impact events. Such *impacting hybrid systems* usually have the property that as the impact velocity goes to zero, the recoil velocity also goes to zero. It follows that for grazing events (i.e. zero-velocity impacts) nearby trajectories stay near each other regardless of whether or not an impact occurs. Such continuity of the flow does not occur for more general hybrid systems such as impulsive systems [21].

Following [9, 39] we consider an impacting hybrid system that in local co-ordinates close to a single impacting surface can be written in the form

$$\begin{aligned} \dot{x} &= F(x; \xi), & \text{for } H(x; \xi) > 0, \\ x &\mapsto R(x; \xi), & \text{for } H(x; \xi) = 0, \end{aligned} \tag{1}$$

where the vector field  $F$ , the reset law  $R$ , and the switching function  $H$  are  $C^k$  functions (with  $k$  sufficient large) of the state variable  $x \in \mathbb{R}^n$  and a parameter vector  $\xi \in \mathbb{R}^m$ . When considering codimension-two bifurcations we shall often choose  $m = 2$  and set  $\xi = (\mu, \eta)$ , where the BEB occurs for  $\mu = 0$ . Where it is unequivocal, we shall sometimes suppress the parameter dependence altogether.

Let us describe the basic features of the dynamics of an impacting hybrid system (1). Figure 1 illustrates the path of a typical trajectory in such a system. The trajectory follows the vector field  $F$  until reaching the switching surface  $\Sigma = \{x \in \mathbb{R}^n \mid H(x) = 0\}$  where it is mapped under  $R$  to a different point on  $\Sigma$  then re-commences evolution under  $F$ .

We assume  $\Sigma = \{x \in \mathbb{R}^n \mid H(x) = 0\}$  is a smooth codimension-one surface, so assume the gradient vector  $\nabla H(x)$  is non-zero at all points on  $\Sigma$ . The direction of  $F(x)$  relative to  $\Sigma$  is governed by the sign of the first Lie derivative

$$v(x) = \mathcal{L}_F H(x) = \nabla H(x)^\top F(x), \tag{2}$$

which is in keeping with mechanical systems we refer to as the velocity with respect to the impact surface.

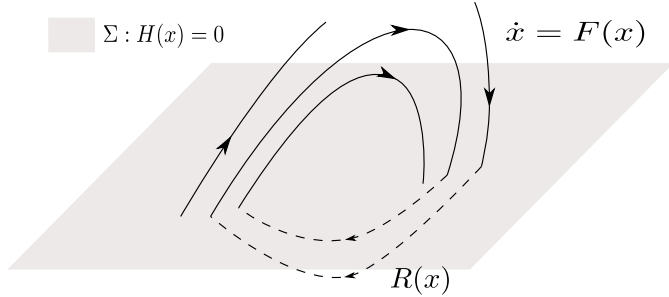


Figure 1: A three-dimensional sketch showing a trajectory of (1) intersecting the switching surface  $\Sigma$  several times.

We use this derivative to partition  $\Sigma$  into three pieces, the *incoming set*  $\Sigma^- = \{x \in \Sigma \mid v(x) < 0\}$ , the *outgoing set*  $\Sigma^+ = \{x \in \Sigma \mid v(x) > 0\}$ , and the *grazing set*  $\Sigma^0 = \{x \in \Sigma \mid v(x) = 0\}$ .

The reset law  $R$  models impact events where the recoil velocity tends to zero as the impact velocity tends to zero. Hence we can write the reset law as

$$R(x) = x + W(x)v(x), \quad (3)$$

where  $W$  is a smooth vector field, so that  $R$  is the identity map on the grazing set. Note that by writing  $v(R(x)) = -r(x)v(x)$ , the quantity  $r(x)$  can be interpreted as a *coefficient of restitution*. We assume  $r(x) > 0$  for all  $x \in \Sigma^- \cup \Sigma^0$  so that the reset law maps  $\Sigma^-$  to  $\Sigma^+$ . It is a simple exercise to show  $r(x) = -1 - \nabla v(x)^\top W(x)$  at any  $x \in \Sigma^0$ . Consequently

$$\nabla v(x)^\top W(x) < -1 \quad (4)$$

at any  $x \in \Sigma^0$  which will be important below.

It is useful to also define the acceleration relative to  $\Sigma$ :

$$a(x) = \mathcal{L}_F^2 H(x) = \nabla v(x)^\top F(x).$$

If a trajectory hits  $\Sigma^0$  at a point where  $a(x) > 0$  then it *grazes*  $\Sigma$  with a quadratic tangency. There is a rich literature on grazing bifurcations in impacting systems via the theory of discontinuity mappings [2, 12, 13, 29].

Points that instead have  $a(x) < 0$  define the *sticking set*

$$\Sigma_-^0 = \{x \in \Sigma^0 \mid a(x) < 0\}.$$

Typically trajectories can only approach  $\Sigma^0$  via the accumulation of an infinite *chattering sequence* of impacts (sometimes referred to as a Zeno phenomenon) [25, 44]. Once such accumulation has occurred, a consistent way within the piecewise-smooth framework to define future evolution is to adapt the Filippov formalism [11] and define the *sticking vector field*

$$F_s(x) = \left( I - \frac{W(x)\nabla v(x)^\top}{\nabla v(x)^\top W(x)} \right) F(x), \quad (5)$$

which is tangent to  $\Sigma^0$ . *Sticking motion* refers to evolution on the codimension-two sticking set  $\Sigma^0$  governed by  $\dot{x} = F_s(x)$ . Notice (5) is well-defined by (4).

This paper concerns bifurcations of equilibria, which, for impacting hybrid systems of the form (1), may be of two types: regular equilibria and pseudo-equilibria. These are zeros of  $F$  and  $F_s$ , respectively, and are valid solutions to (1) if they are ‘admissible’, as defined below.

**Definition 1.** *A regular equilibrium is a point  $x^* \in \mathbb{R}^n$  for which  $F(x^*) = 0$ ; it is admissible if  $H(x^*) > 0$ , virtual if  $H(x^*) < 0$ , and a boundary equilibrium if  $H(x^*) = 0$ . A pseudo-equilibrium is a point  $x^* \in \Sigma^0$  for which  $F_s(x^*) = 0$ ; it is admissible if  $a(x^*) < 0$ , and virtual if  $a(x^*) > 0$ .*

## 2.1 Boundary equilibrium bifurcations

As the parameter vector  $\xi$  of an impacting hybrid system (1) is varied, a boundary equilibrium bifurcation (BEB) occurs when a regular equilibrium  $x^*(\xi)$  collides with the switching surface  $\Sigma$ . At the bifurcation,  $x^*$  is a boundary equilibrium, and also a pseudo-equilibrium with  $a(x^*) = 0$  because all the Lie derivatives  $\mathcal{L}_F^i H(x^*)$ , for  $i = 1, 2, \dots$ , are zero.

Consequently BEBs can be thought of as a transition between regular and pseudo-equilibria, and generically this transition conforms to one of two cases [3]. In both cases the equilibria are unique, locally, and each is admissible on one side of the bifurcation and virtual on the other side of the bifurcation. If they are admissible on different sides of the bifurcation the BEB is referred as *persistence* because if we only consider admissible features of the dynamics then a single equilibrium is seen to persist. If instead the equilibria are admissible on the same side of the bifurcation the BEB is referred to as a *nonsmooth fold* because, with the same mindset, two equilibria are seen to collide and annihilate much like a saddle-node bifurcation or fold.

While a complete characterisation of equilibria near generic BEBs is available, except for two-dimensional systems [3] there is very little theory on the existence and

nature of other invariant sets that can be created in BEBs. Recent work of two of the authors [39] gave sufficient conditions for single-impact limit cycles to be born at a BEB, and a method to analyse their stability. In particular it was found that for systems with more than two dimensions, multiple limit cycles can be born at a BEB and a stable limit cycle can coexist with an admissible stable pseudo-equilibrium. This motivates the present study on codimension-two bifurcations that change the number of limit cycles being born at a BEB.

Consider a system (1) with parameter vector  $\xi = (\mu, \eta) \in \mathbb{R}^2$  that undergoes a BEB when  $\mu = 0$  for all values of  $\eta$  (which later will be used to unfold codimension-two points). For simplicity, suppose near-identity transformations have been made to flatten the switching surface  $\Sigma$  so that the switching function  $H$  can be written as

$$H(x; \mu, \eta) = C^\top x,$$

for a constant  $n \times 1$  vector  $C$ . Since the vector fields  $F$  and  $W$  are smooth, where  $W$  appears in the reset law via (3), and  $F(0; 0, \eta) = 0$  for all  $\eta$ , we can write

$$\begin{aligned} F(x; \mu, \eta) &= A(\eta)x + M(\eta)\mu + \mathcal{O}((\|x\| + |\mu|)^2), \\ W(x; \mu, \eta) &= -B(\eta) + \mathcal{O}(\|x\| + |\mu|), \end{aligned} \quad (6)$$

where  $A \in \mathbb{R}^{n \times n}$  and  $B, M \in \mathbb{R}^n$  are smooth functions of  $\eta$ . By substituting these into our earlier formulas, we obtain

$$R(x; \mu, \eta) = (I - BC^\top A)x - BC^\top M\mu + \mathcal{O}((\|x\| + |\mu|)^2). \quad (7)$$

If  $A$  is invertible, then, locally, (1) has a unique regular equilibrium at

$$x_{\text{reg}}(\mu, \eta) = -A^{-1}M\mu + \mathcal{O}(\mu^2). \quad (8)$$

This equilibrium is admissible if  $H(x_{\text{reg}}(\mu, \eta); \mu, \eta) > 0$ , where

$$H(x_{\text{reg}}(\mu, \eta); \mu, \eta) = -C^\top A^{-1}M\mu + \mathcal{O}(\mu^2). \quad (9)$$

The eigenvalues associated with  $x_{\text{reg}}$  are  $O(\mu)$  perturbations of the eigenvalues of  $A$ . So if all eigenvalues of  $A$  have negative real part, then  $x_{\text{reg}}$  is admissible and asymptotically stable for all sufficiently small values of  $\mu$  with the sign of  $\mu$  opposite to the sign of  $C^\top A^{-1}M$ .

By substituting the series (6) into the sticking vector field (5), we obtain

$$F_s(x) = \left( I - \frac{BC^\top A}{C^\top AB} \right) (Ax + M\mu) + \mathcal{O}((\|x\| + |\mu|)^2), \quad (10)$$

where  $C^\top AB > 0$  (because  $\nabla v(x)^\top W(x) < 0$  at points on  $\Sigma^0$ , see (4)). The Jacobian matrix of  $F_s$  at  $(x; \mu) = (0; 0)$  is

$$A_s = \left( I - \frac{BC^\top A}{C^\top AB} \right) A.$$

This matrix has a zero eigenvalue with algebraic multiplicity at least two (because the codimension-two sticking set is invariant under  $F_s$ ). If the algebraic multiplicity is exactly two (as is generically the case), then, locally, (1) has a unique pseudo-equilibrium  $x_{\text{ps}}(\mu, \eta)$  with  $x_{\text{ps}}(0, \eta) = 0$  for all  $\eta$ . By definition 1 the pseudo-equilibrium is admissible if  $a(x_{\text{ps}}(\mu, \eta); \mu, \eta) < 0$ , and after routine algebraic manipulation [3] we obtain

$$a(x_{\text{ps}}(\mu, \eta); \mu, \eta) = \frac{C^\top ABC^\top A^{-1}M}{C^\top A^{-1}B} \mu + \mathcal{O}(\mu^2). \quad (11)$$

If we restrict our attention to the sticking set, then the eigenvalues associated with  $x_{\text{ps}}$  are the  $n - 2$  non-zero eigenvalues of  $A_s$ . These are the eigenvalues of an  $(n - 2) \times (n - 2)$  matrix  $\hat{A}_s$  defined as the Jacobian matrix of the restriction of  $F_s$  to the sticking set. So if all eigenvalues of  $\hat{A}_s$  have negative real part, then  $x_{\text{reg}}$  is an asymptotically stable equilibrium of  $F_s$  on  $\Sigma_0$ .

The signs of (9) and (11) determine the admissibility of the equilibria, so we can use the coefficients of their leading order terms to classify the BEB as persistence or a nonsmooth fold.

**Theorem 1** ([3]). *Consider an impacting hybrid system (1) written with (6). Suppose  $A$  is non-singular,  $C^\top AB > 0$ , and  $C^\top A^{-1}M \neq 0$ . If  $C^\top A^{-1}B < 0$  the BEB at  $\mu = 0$  corresponds to persistence, while if  $C^\top A^{-1}B > 0$  it is a nonsmooth fold.*

## Remarks

1. The proof of Theorem 1 is based on a co-ordinate *blow-up* that leads to a scale-invariant normal form. Specifically, for small  $\mu \neq 0$ , under  $y = \frac{x}{\mu}$  the system (1) becomes, to leading order,

$$\begin{aligned} \dot{y} &= Ay + M\sigma, & \text{for } C^\top y > 0, \\ y &\mapsto (I - BC^\top A)y - BC^\top M\sigma, & \text{for } C^\top y = 0, \end{aligned} \quad (12)$$

where  $\sigma = \text{sign}(\mu)$ . Thus, to leading order, the dynamics near a BEB are scale invariant for each sign of  $\mu$ . In what follows, we describe scenarios that require us to go beyond this leading-order form; nevertheless, the blown-up co-ordinate  $y$  will prove invaluable.



2. The basic classification provided by theorem 1 is intimately connected to the stability of the equilibria. In particular, we find [3, Eq. 50]

$$\det(\hat{A}_s) = -\frac{C^\top A^{-1}B}{C^\top AB} \det(A). \quad (13)$$

So if both equilibria are asymptotically stable, then all eigenvalues of  $A$  and  $\hat{A}_s$  have negative real part, thus  $\det(A)$  and  $\det(\hat{A}_s)$  have the same sign (they are both negative if  $n$  is odd and both positive if  $n$  is even). In this case  $C^\top A^{-1}B < 0$  because  $C^\top AB > 0$ , so the boundary equilibrium bifurcation corresponds to persistence. More generally (13) allows us to classify the bifurcation from the number of positive eigenvalues of  $A$  and  $\hat{A}_s$ , as done originally by Feigin [10] for a related non-smooth bifurcation of maps.

Next we consider limit cycles of (1).

## 2.2 Single-impact limit cycles

Suppose an impacting hybrid system (1) has a single-impact period- $T$  limit cycle. This limit cycle corresponds to a point  $x^* \in \Sigma^+$  satisfying

$$x^* = \varphi(R(x^*), T), \quad \text{with } H(\varphi(R(x^*), t)) \neq 0, \text{ for all } 0 < t < T, \quad (14)$$

where  $\varphi$  denotes the flow of the vector field  $F$ . The stability of the limit cycle can be determined from the derivative of  $\varphi(R(x), T)$ , which can be evaluated by multiplying a *saltation matrix* with the monodromy matrix associated with  $F$ , [3, 39].

In [39] we showed how to convert the problem of the existence of such a limit cycle of the truncated form (12) into an eigenproblem involving the matrix exponential  $\exp(AT)$ . Here we treat the general system (1) and relate limit cycles to fixed points of a Poincaré map. Care is needed to ensure the map is well-defined arbitrarily close to the BEB at  $\mu = 0$  where the limit cycle shrinks to a point, and we use blown-up coordinates to achieve this.

Without loss of generality, let us consider limit cycles on the  $\mu > 0$  side of the BEB. Again we use the blow-up

$$y = \frac{x}{\mu}, \quad (15)$$

that for  $\mu > 0$  converts (1) to the form

$$\begin{aligned} \dot{y} &= Ay + M + \mathcal{O}(\mu), & \text{for } C^\top y > 0, \\ y &\mapsto (I - BC^\top A)y - BC^\top M + \mathcal{O}(\mu), & \text{for } C^\top y = 0. \end{aligned} \quad (16)$$

Unlike in (12) we have not truncated, so (16) is conjugate to (1) for  $\mu > 0$ . But although (16) was constructed subject to the assumption  $\mu > 0$ , *functionally* it is well-defined and can be extended smoothly for all values of  $\mu$  in a neighborhood of 0. This observation is crucial as it allows us to use the implicit function theorem in the proofs below. Note, we use tildes for quantities ( $F$ ,  $H$ ,  $\Sigma$  etc) defined in terms of  $y$  rather than  $x$ .

Let  $Q$  be an  $(n - 1) \times n$  matrix with the property that

$$S = \begin{bmatrix} C^\top \\ Q \end{bmatrix}$$

is invertible. Then  $u = \zeta(y) = Qy$  is a bijection from  $\tilde{\Sigma}$  to  $\mathbb{R}^{n-1}$ . Next we define

$$\Pi^- = \zeta(\tilde{\Sigma}^-), \quad \Pi^+ = \zeta(\tilde{\Sigma}^+), \quad \Pi^0 = \zeta(\tilde{\Sigma}^0),$$

and a Poincaré map  $P : \Pi^+ \rightarrow \Pi^+$  for the system (16) by

$$P(u; \mu, \eta) = \zeta(\tilde{R}(y^-)), \tag{17}$$

where  $y^-$  is the first point at which the forward orbit of  $\zeta^{-1}(u) \in \tilde{\Sigma}^+$  under  $\tilde{F}$  reaches  $\tilde{\Sigma}^-$ , assuming it ever does so. This is illustrated in Figure 2. If  $\hat{u}$  is a fixed point of  $P$

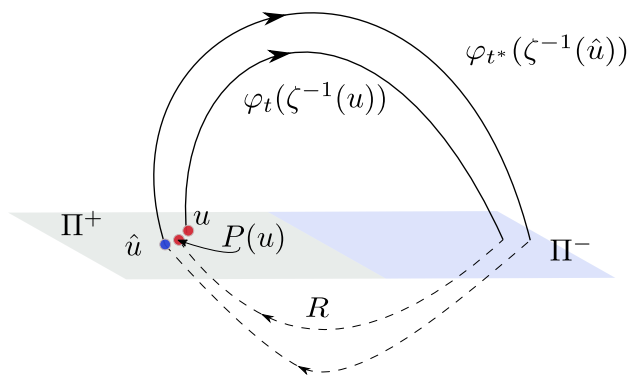


Figure 2: A three-dimensional sketch illustrating the action of the Poincaré map  $P$ , defined by (17). A fixed point  $\hat{u}$  of  $P$  with  $\mu > 0$  corresponds to a limit cycle of (1).

with  $\mu > 0$ , then  $x^* = \mu\zeta^{-1}(\hat{u}) \in \Sigma^+$  belongs to a single-impact periodic orbit of (1). The eigenvalues of the Jacobian matrix  $DP(u)$  are the non-trivial Floquet multipliers of the periodic orbit. The following technical result shows that  $P$  is smooth.

**Lemma 1.** *Suppose  $F$  and  $R$  in (1) are  $C^k$  ( $k \geq 2$ ). If  $P$  is well-defined at  $(u_0; \mu_0, \eta_0)$ , where  $u_0 \in \Pi^+$ ,  $\mu_0 \in \mathbb{R}$ , and  $\eta_0 \in \mathbb{R}$ , then it is well-defined and  $C^{k-1}$  in a neighbourhood of  $(u_0; \mu_0, \eta_0)$ .*

*Proof.* The scaled system (16) is  $C^{k-1}$  because we have divided by  $\mu$ , so the vector field  $\tilde{F}$  admits a  $C^{k-1}$  flow  $\varphi(y, t; \mu, \eta)$  [1]. Thus  $J(y, t; \mu, \eta) = \tilde{H}(\varphi(y, t; \mu, \eta))$  is a  $C^{k-1}$  function. Let  $y^+ = \zeta^{-1}(u_0)$  and  $\tau$  be the evolution time between  $y^+$  and  $y^-$  belonging to  $\tilde{\Sigma}^-$ . That is,  $y^- = \varphi(y^+, \tau; \mu_0, \eta_0)$ , and so  $J(y^+, \tau; \mu_0, \eta_0) = 0$ . Observe  $\frac{\partial J}{\partial t}(y^+, \tau; \mu_0, \eta_0) = \nabla \tilde{H}(y^-)^\top \tilde{F}(y^-; \mu_0, \eta_0)$  is negative because  $y^-$  belongs to  $\tilde{\Sigma}^-$ . Thus, locally, we can solve  $J(y, t; \mu, \eta) = 0$  for  $t$ : by the implicit function theorem there exists a unique  $C^{k-1}$  function  $T$  defined on a neighbourhood  $\mathcal{U}$  of  $(y^+; \mu_0, \eta_0)$  such that  $J(y, T(y; \mu, \eta); \mu, \eta) = 0$  for all  $(y; \mu, \eta) \in \mathcal{U}$ . So the forward orbit of any such  $y$  under  $\tilde{F}$  returns to  $\tilde{\Sigma}$  at the point  $\varphi(y, T(y; \mu, \eta); \mu, \eta)$ . Moreover, we can assume  $\mathcal{U}$  has been taken small enough that this is the first point at which the orbit returns to  $\tilde{\Sigma}$ . So for any  $(u; \mu, \eta)$  such that  $(\zeta^{-1}(u); \mu, \eta) \in \mathcal{U}$ , the Poincaré map  $P(u; \mu, \eta)$  is well-defined and  $P(u; \mu, \eta) = \zeta\left(\tilde{R}(\varphi(y, T(y; \mu, \eta); \mu, \eta))\right)$ , where  $y = \zeta^{-1}(u)$ . Thus  $P$  is  $C^{k-1}$  because we have expressed it as a composition of  $C^{k-1}$  functions.  $\square$

In summary we have reduced questions of existence and stability of single-impact limit cycles to those of fixed points of a Poincaré map  $P$ . Importantly  $P$  is smooth so we can employ classical (smooth) bifurcation theory to analyse bifurcations of the limit cycles.

### 3 Main results

We shall now assume that a fixed point of  $P$ , defined by (17) exists at parameter values  $(\mu, \eta) = (0, 0)$ . As discussed above,  $P$  is well-defined and smooth for all values of  $\mu$  in a neighbourhood of 0 even though it only corresponds to dynamics of (1) for  $\mu > 0$ , where this choice of sign was taken without loss of generality. We then allow  $\eta$  to unfold a degeneracy in the linearization about this fixed point.

#### 3.1 BEB-saddle-node bifurcation

We first consider the case where the Poincaré map  $P$  has a fixed point with stability multiplier 1 at  $(\mu, \eta) = (0, 0)$ . Such a multiplier suggests the occurrence of a saddle-node bifurcation, and indeed the theorem below explains the existence of a curve of saddle-node bifurcations of limit cycles for the original system (1).

**Theorem 2.** *Suppose  $F$  and  $R$  in (1) are  $C^k$  ( $k \geq 3$ ) and  $P(u; 0, 0)$  has a fixed point  $\hat{u}$ . Suppose  $DP(\hat{u}; 0, 0)$  has an eigenvalue 1 of algebraic multiplicity one and no other eigenvalues with unit modulus. Let  $w \in \mathbb{R}^{n-1}$  and  $v \in \mathbb{R}^{n-1}$  be left and right eigenvectors, respectively, for the eigenvalue 1 with  $w^\top v = 1$  and suppose*

$$w^\top \frac{\partial P}{\partial \eta} \neq 0, \quad (18)$$

$$w^\top [(D^2P)(v, v)] \neq 0. \quad (19)$$

*Then there exists  $\delta > 0$  and a  $C^{k-2}$  function  $g : (-\delta, \delta) \rightarrow \mathbb{R}$  with  $g(0) = 0$  such that (1) has saddle-node bifurcations of single-impact limit cycles on  $\eta = g(\mu)$  for all  $0 < \mu < \delta$ .*

The codimension-two point  $(\mu, \eta) = (0, 0)$  is characterized by the BEB at  $\mu = 0$  and the eigenvalue 1 associated with the bifurcating limit cycle at  $\eta = 0$ . Theorem 2 contains several genericity conditions to ensure saddle-node bifurcations arise. The eigenvalue 1 needs to be a simple eigenvalue and there cannot be any other eigenvalues with unit modulus. The *transversality condition* (18) ensures  $\eta$  unfolds the bifurcation in a generic fashion. The *non-degeneracy condition* (19) ensures  $P$  has the required nonlinearity to support the creation of two limit cycles. These conditions appear in the classical saddle-node bifurcation theorem for maps [20, pg. 148]. In the proof below we in fact obtain a formula for  $g'(0)$  in terms of the derivatives of the restriction of  $P$  to a centre manifold.

*Proof.* Since  $P$  is smooth (lemma 1) classical (smooth) bifurcation theory can be employed. The map  $P$  has a  $C^{k-1}$  centre manifold through  $\hat{u}$  with local representation  $u = h(s; \mu, \eta)$ , where  $s \in \mathbb{R}$ . Let  $\hat{s} \in \mathbb{R}$  be such that  $\hat{u} = h(\hat{s}; 0, 0)$ . Let  $p(s; \mu, \eta)$  denote the restriction of  $P$  to the centre manifold, and let  $q(z; \mu, \eta)$  denote this map under the translation  $z = s - \hat{s}$ . Then  $q$  is  $C^{k-1}$  and has the form

$$q(z; \mu, \eta) = z + a\mu + b\eta + cz^2 + d\mu z + e\eta z + m\mu^2 + n\eta^2 + \text{H.O.T.}, \quad (20)$$

where  $a, b, c, d, e, m, n \in \mathbb{R}$  and H.O.T. contains all cubic and higher order terms. Notice the coefficient of the  $z$ -term in (20) is 1 due to the assumption that  $\hat{u}$  has a stability multiplier of 1. Following [28, pg. 174] we have

$$a = w^\top \frac{\partial P}{\partial \mu}, \quad b = w^\top \frac{\partial P}{\partial \eta}, \quad c = \frac{1}{2} w^\top [(D^2P)(v, v)], \quad (21)$$

while formulas for  $d$ ,  $e$ ,  $m$  and  $n$  are not needed for this proof but are given in appendix A as they are important when unfolding the bifurcation (see instead appendix B.1). Note that  $b \neq 0$  by (18) and  $c \neq 0$  by (19). Since  $b \neq 0$ , locally we can

solve the fixed point equation  $z = q(z; \mu, \eta)$  for  $\eta$  giving

$$\eta = g_1(\mu, z) = -\frac{a}{b}\mu - \frac{c}{b}z^2 + \text{H.O.T.},$$

which is  $C^{k-1}$  by the implicit function theorem. The derivative of  $q$  is

$$\frac{\partial q}{\partial z}(z; \mu, \eta) = 1 + 2cz + \text{H.O.T.},$$

which is  $C^{k-2}$ . Since  $c \neq 0$ , locally we can solve  $\frac{\partial q}{\partial z}(z; \mu, g_1(\mu, z)) = 1$  for  $z$  giving

$$z = g_2(\mu) = \mathcal{O}(\mu),$$

which is  $C^{k-2}$  by the implicit function theorem. Thus, saddle-node bifurcations occur on

$$\eta = g_1(\mu, g_2(\mu)) = -\frac{a}{b}\mu + \mathcal{O}(\mu^2). \quad (22)$$

□

### 3.2 BEB-period-doubling bifurcations

The following result is a natural analogue of the previous theorem for the case of a multiplier  $-1$  at  $\eta = 0$ . The transversality and non-degeneracy conditions are now (23) and (24) respectively. The latter condition appears in the classical period-doubling bifurcation theorem and ensures a period-doubled solution is created in a generic fashion. A derivation of (24) is provided by Kuznetsov [28, pgs. 184–185]. In Appendix A we provide explicit formulas for the constants in (24) in terms of  $P$  and its derivatives.

**Theorem 3.** *Suppose  $F$  and  $R$  in (1) are  $C^k$  ( $k \geq 4$ ) and  $P(u; 0, 0)$  has a fixed point  $\hat{u}$ . Suppose  $DP(\hat{u}; 0, 0)$  has an eigenvalue  $-1$  of algebraic multiplicity one and no other eigenvalues with unit modulus. Locally the fixed point persists having a  $C^{k-1}$  eigenvalue  $\lambda(\mu, \eta)$  with  $\lambda(0, 0) = -1$ ; suppose*

$$\frac{\partial \lambda}{\partial \eta}(0, 0) \neq 0. \quad (23)$$

and

$$c^2 + f \neq 0, \quad (24)$$

where  $c$  and  $f$  are the coefficients of quadratic and cubic terms, respectively, of the restriction of  $P$  to the centre manifold. Then there exists  $\delta > 0$  and a  $C^{k-2}$  function  $g : (-\delta, \delta) \rightarrow \mathbb{R}$  with  $g(0) = 0$  such that (1) has period-doubling bifurcations of single-impact limit cycles on  $\eta = g(\mu)$  for all  $0 < \mu < \delta$ .

*Proof.* As in the proof of theorem 2 we restrict  $P$  to a one-dimensional centre manifold and move the critical fixed point to the origin resulting in a map of the form

$$q(z; \mu, \eta) = -z + a\mu + b\eta + cz^2 + d\mu z + e\eta z + fz^3 + \text{H.O.T.}, \quad (25)$$

where  $a, b, c, d, e, f \in \mathbb{R}$  and H.O.T. contains all terms that are quadratic in  $\mu$  and  $\eta$  and all cubic and higher order terms except the  $z^3$ -term which has been written explicitly because it is important below. Let  $w \in \mathbb{R}^{n-1}$  and  $v \in \mathbb{R}^{n-1}$  be left and right eigenvectors, respectively, for the eigenvalue  $-1$  and satisfying  $w^\top v = 1$ . Again,  $a, b$ , and  $c$  are given explicitly by (21). The coefficients  $d, e$  and  $f$  are slightly harder to compute, as they rely on careful consideration of the parameter dependence of the various co-ordinate transformations. A full derivation is given in appendix A. Note that these terms play a role in the unfolding of the dynamics, and ignoring them can alter the criticality of the various bifurcating orbits, and they are important in making asymptotic predictions for the amplitudes of bifurcating orbits (see appendix B).

By the implicit function theorem, locally there is a unique  $C^{k-1}$  fixed point

$$z = g_1(\mu, \eta) = \frac{a}{2}\mu + \frac{b}{2}\eta + \mathcal{O}((|\mu| + |\eta|)^2).$$

The stability multiplier of this fixed point is

$$\lambda(\mu, \eta) = \frac{\partial q}{\partial z}(g_1(\mu, \eta); \mu, \eta) = -1 + (ac + d)\mu + (bc + e)\eta + \mathcal{O}((|\mu| + |\eta|)^2),$$

which is  $C^{k-2}$ . We have  $bc + e \neq 0$ , by the transversality condition (23), so, by the implicit function theorem, locally the stability multiplier is  $-1$  on a  $C^{k-2}$  curve

$$\eta = g_2(\mu) = -\frac{ac + d}{bc + e}\mu + \mathcal{O}(\mu^2). \quad (26)$$

For sufficiently small values of  $\mu$ , period-doubled solutions are created on this curve because the non-degeneracy condition (24) is satisfied.  $\square$

## 4 Numerical verification

In this section we perform bifurcation analyses on examples to illustrate the unfoldings predicted by theorems 2 and 3. We evaluate the coefficients in the one-dimensional forms (20) and (25) and use (22) and (26) to determine the slope of the saddle-node and period-doubling bifurcation curves at the codimension-two points, and compare these to the results of numerical continuation.

## 4.1 Numerical computation of the normal form coefficients

We first provide general comments on the manner by which the coefficients in (20) and (25) can be computed. If the vector field  $F$  in (1) is linear, these coefficients can be computed analytically. This is because the flow can be expressed explicitly as a matrix exponential, from which we can find explicit expressions for the Poincaré map  $P$  up to an implicit transcendental equation for the evolution time  $T$ . Care is needed when evaluating the derivatives of  $P$  because  $T$  varies with the initial point and this needs to be accounted for when differentiating. Note that even though  $F$  is in this case linear,  $P$  will be nonlinear and satisfies the non-degeneracy conditions (19) and (24) in generic situations. If instead  $F$  is nonlinear,  $P$  needs to be evaluated numerically and its derivatives can be computed using linear variational equations or finite differences.

For linear vector fields  $F$  in the examples below, limit cycles in blown-up coordinates were computed using the semi-analytic continuation method developed in [39]. For nonlinear  $F$  they were computed from direct numerical simulations of the system.

In this section codimension-two points are identified as follows. We vary a second parameter and solve numerically to find a value of this parameter at which  $P$  has a fixed point with stability multiplier 1 or  $-1$  in the limit  $\mu \rightarrow 0^+$  (flipping the sign of  $\mu$  if needed). This limit is evaluated by working in blown-up coordinates (15) and setting  $\mu = 0$ . We shift the second parameter so that the codimension-two point occurs at 0, and call it  $\eta$  so that theorems 2 and 3 can be applied directly. We then compute the critical eigenvectors  $w$  and  $v$  and the coefficients in (20) and (25) as discussed above. We can also use formulas obtained in the above proofs to approximate the amplitude of the bifurcating limit cycles. Details of these calculations are provided in Appendices A and B.

All computations were carried out in MATLAB and the code is available at <https://github.com/HongTang973>. In what follows we write  $\mathbf{e}_i$ , where  $i = 1, 2, 3, \dots$ , for the  $i^{\text{th}}$  standard basis vector of  $\mathbb{R}^n$ .

## 4.2 Three-dimensional systems

We start by considering three-dimensional systems (1) where the reset law has the form (3) and  $F$ ,  $W$ , and  $H$  are truncated from eq. (6) with the form

$$\begin{aligned} F(x; \mu, \eta) &= A\eta x + M\mu + A_1\mu x + \epsilon(q_1x_1x_2 + q_2x_1x_3)\mathbf{e}_1, \\ W(x; \mu, \eta) &= -B, \\ H(x; \mu, \eta) &= C^\top x, \end{aligned} \tag{27}$$

where  $A, A_1 \in \mathbb{R}^{3 \times 3}$ ,  $B, C, M \in \mathbb{R}^3$ , and  $q_1, q_2, \epsilon \in \mathbb{R}$ . We first consider cases where  $F$  is linear, i.e.  $\epsilon = 0$ , then show that the same phenomenon occurs when  $F$  is nonlinear. The term  $A_1 \mu x$  (higher order in eq. (6)) provides additional  $\mu$ -dependency.

#### 4.2.1 BEB-saddle-node bifurcations

**Example 4.1.** *Suppose the coefficients in (27) have the form*

$$A = \begin{bmatrix} t & 1 & 0 \\ m & 0 & 1 \\ d & 0 & 0 \end{bmatrix}, \quad B = \begin{bmatrix} 0 \\ b_2 \\ b_3 \end{bmatrix}, \quad C = \mathbf{e}_1, \quad M = -\mathbf{e}_3, \quad A_1 = -\mathbf{e}_1^\top \mathbf{e}_1, \quad (28)$$

where  $t, m, d, b_2, b_3 \in \mathbb{R}$ . Since  $A$  is a companion matrix (cf. [39]), its parameters are given in terms of its eigenvalues  $\lambda_1, \lambda_2$ , and  $\lambda_3$  by

$$t = \lambda_1 + \lambda_2 + \lambda_3, \quad m = -\lambda_1 \lambda_2 - \lambda_1 \lambda_3 - \lambda_2 \lambda_3, \quad d = \lambda_1 \lambda_2 \lambda_3.$$

We set the eigenvalues as

$$\lambda_1 = -0.1 + 0.2i, \quad \lambda_2 = -0.1 - 0.2i, \quad \lambda_3 = -0.5.$$

and fix  $b_3 = 1.6$  and  $\epsilon = 0$  and use  $b_2$  as the second bifurcation parameter. ■

The key quantities in theorem 1 are

$$C^\top AB = b_2, \quad C^\top A^{-1}B = \frac{b_3}{d}, \quad C^\top A^{-1}M = -\frac{1}{d},$$

so with  $b_2 > 0$  the BEB at  $\mu = 0$  corresponds to persistence.

Numerically we found that  $P$  in the limit  $\mu \rightarrow 0^+$  has a fixed point with stability multiplier 1 when  $b_2 = b_2^0 \approx 1.7819$ , and the assumptions of theorem 2 hold using  $\eta = b_2 - b_2^0$ . for  $\mu > 0$  saddle-node bifurcations occur on Thus a curve  $b_2 = b_2^0 + g(\mu)$  with  $g(0) = 0$ . We computed this curve numerically and it is shown in Figure 3a. Also as a dashed line we show the theoretical linear approximation  $b_2 = b_2^0 - \frac{a}{b}\mu$ , due to eq. (22), where  $a \approx 0.1695$  and  $b \approx -0.0391$  for this example. As expected, the slope  $-\frac{a}{b}$  appears to match that of the numerically computed curve at the codimension-two point.

The BEB and saddle-node bifurcation curves divide the parameter plane locally into three regions. For  $\mu < 0$  the system has a stable regular equilibrium (RE), for



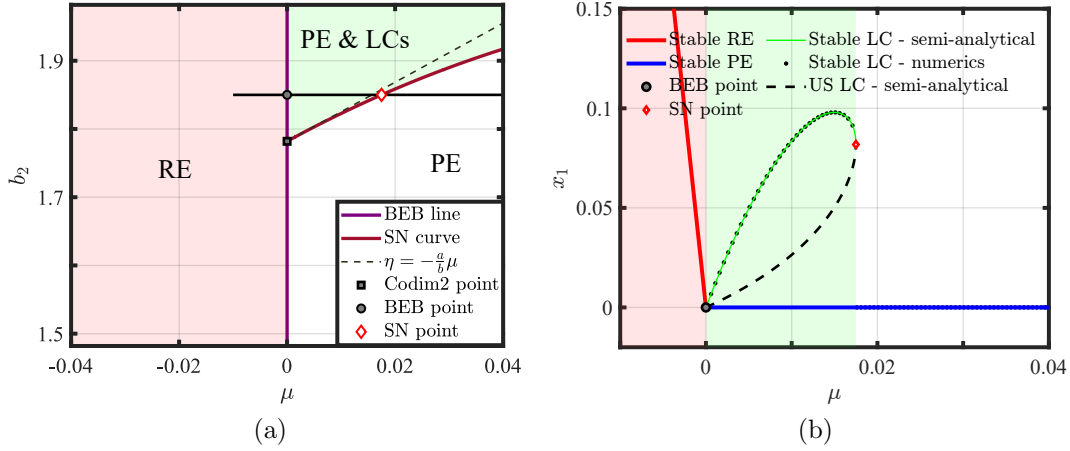


Figure 3: (a) A two-parameter bifurcation diagram for example 4.1 (RE: regular equilibrium; PE: pseudo-equilibrium; LC: limit cycle; SN: saddle-node bifurcation; BEB: boundary equilibrium bifurcation). (b) A one-parameter slice along the horizontal line at  $b_2 = 1.85$  shown in panel (a).

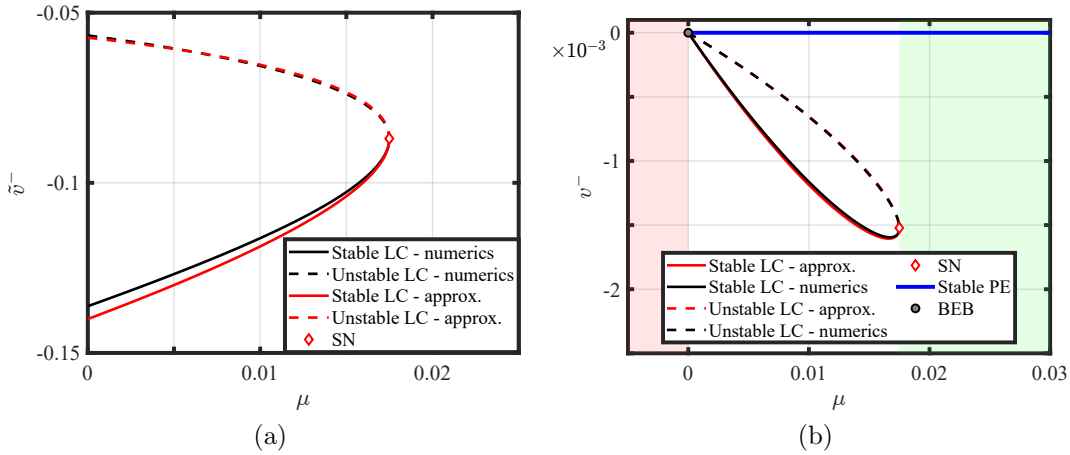


Figure 4: (a) A comparison of the impact velocities of the limit cycles in blown-up co-ordinates computed numerically (black) and via the normal-form approximation (red), using  $b_2 = 1.85$  as in Figure 3b. (b) The same quantities in original co-ordinates; the blue line denotes the stable pseudo-equilibrium.

$\mu > 0$  below the saddle-node curve it has a stable pseudo-equilibrium (PE), while for  $\mu > 0$  above the saddle-node curve it has a stable pseudo-equilibrium and stable

and unstable single-impact limit cycles (LCs).

Figure 3b shows a bifurcation diagram for a one-parameter slice through both bifurcation curves defined by fixing  $b_2 = 1.85$ . This shows the  $x_1$ -values of the regular and pseudo equilibria and the maximum  $x_1$ -values attained by the stable and unstable limit cycles. The limit cycles grow asymptotically linearly from the BEB at  $\mu = 0$ , then collide and annihilate in the saddle-node bifurcation at  $\mu_{\text{SN}} = g^{-1}(b_2 - b_2^0) \approx 0.0175$ . To produce Figure 3b the stable limit cycle was continued numerically, while both stable and unstable limit cycles were continued semi-analytically via the method in [39] (one point on the limit cycle was obtained by solving an eigenproblem, then numerical integration carried out to obtain the maximum  $x_1$ -value of the limit cycle).

Next, we examine the impact velocities of the limit cycles. These are shown in Figure 4a in blown-up coordinates and in Figure 4b in original coordinates. That is, Figure 4b shows the velocity  $v^- = \nabla H(x)^\top F(x)$  evaluated at the point  $x$  at which the limit cycle returns to the switching surface, and Figure 4a shows  $\tilde{v}^- = \frac{v^-}{\mu}$ . As shown in appendix B, the impact velocities are well approximated by

$$\mathcal{A} = \mu \left( \ell_0 + \ell_1 \mu \pm L_{10} \sqrt{-\frac{a(\mu - \mu_{\text{SN}})}{c} + \frac{(d^2 - 4mc)(\mu - \mu_{\text{SN}})^2}{4c^2} - \frac{d(\mu - \mu_{\text{SN}})}{2c}} \right), \quad (29)$$

where  $a$ ,  $c$ ,  $d$  and  $m$  are coefficients in the map (20) on the centre manifold, and  $\ell_0$  and  $\ell_1$  are appropriate coefficients for converting the position on the centre manifold to the impact velocity. We obtained  $a \approx 0.1695$ ,  $b \approx -0.0391$ ,  $c \approx -1.3833$ ,  $d \approx -5.2939$ ,  $e \approx -0.0737$ ,  $m \approx 4.5852$ ,  $\ell_0 \approx -0.0870$ ,  $\ell_1 = 0$  and  $L_{10} \approx 0.1544$ , by numerically evaluating derivatives of  $P$  at the codimension-two point  $(\mu, \eta) = (0, 0)$ . The resulting approximations to the impact velocities are shown in Figure 4 and seen to match well to those obtained via direct integration. A better match can be achieved by evaluating the coefficients at the saddle-node bifurcation  $(\mu, \eta) = (\mu_{\text{SN}}, 1.85)$ .

**Example 4.2.** *Suppose the coefficients are as in example 4.1, except*

$$(a). \quad q_1 = -1, \quad q_2 = 0; \quad (b). \quad q_1 = 0, \quad q_2 = 1;$$

*and we allow various values of  $\epsilon \geq 0$ .*

■

expansion Now with  $\epsilon \neq 0$  the vector field  $F$  is nonlinear. The location of the codimension-two point is unchanged from example 4.1 because the nonlinear terms contribute order- $\mu$  perturbations to the system in blown-up co-ordinates. The nonlinear terms do affect the slope  $-\frac{a}{b}$  of the curve of saddle-node bifurcations. This

explains fig. 5 which shows that for small  $\eta = b_2 - b_2^0 > 0$  two limit cycles are created in the BEB at  $\mu = 0$ , but the location of the saddle-node bifurcation where these are destroyed depends on the value of  $\epsilon$ .

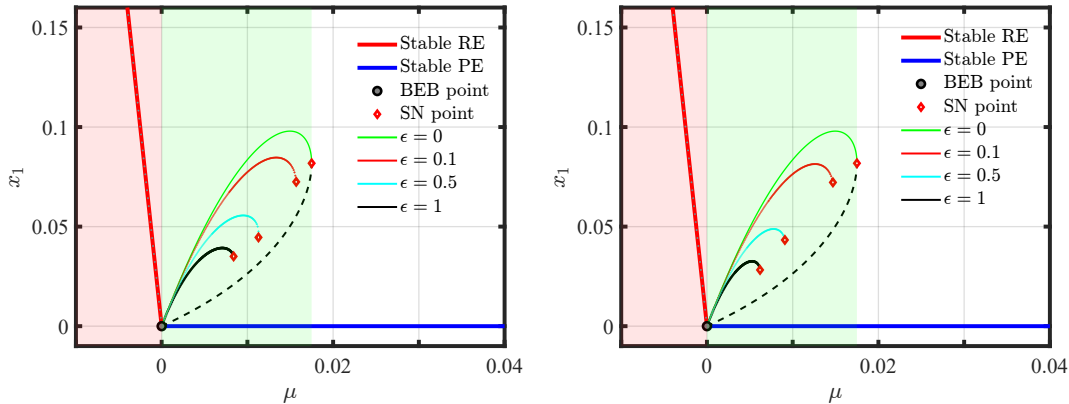


Figure 5: One-parameter bifurcation diagrams for example 4.2 with  $b_2 = 1.85$  and various values of  $\epsilon \geq 0$ . Panel (a) uses  $q_1 = -1$  and  $q_2 = 0$ , while panel (b) uses  $q_1 = 0$  and  $q_2 = 1$ .

#### 4.2.2 BEB-period-doubling bifurcations

**Example 4.3.** *Inspired by forthcoming research into Shilnikov chaos arising from a codimension-three BEB [30], suppose the coefficients in (27) have the form*

$$A = \begin{bmatrix} \rho & \omega & 0 \\ -\omega & \rho & 1 \\ 0 & 0 & -\lambda \end{bmatrix}, \quad A_1 = \mathbf{e}_3^\top \mathbf{e}_3, \quad M = \mathbf{e}_3, \quad C = \mathbf{e}_1, \quad B = [0, 1 + r, -\sigma]^\top.$$

where  $\sigma$  is a new parameter unrelated to that in eq. (12). We fix  $\epsilon = 0$  and

$$\rho = 0.1, \quad \omega = 1, \quad \lambda = 0.3, \quad (30)$$

and consider various values of  $r$  and  $\sigma$ .

■

For this example

$$C^\top AB = (1 + r)\omega, \quad C^\top A^{-1}B = \frac{\omega(\sigma - \lambda(1 + r))}{\lambda(\omega^2 + \rho^2)}, \quad C^\top A^{-1}M = \frac{-\omega}{\lambda(\omega^2 + \rho^2)}.$$

With  $\sigma = \sigma_0 = 0.8$  we found numerically that  $P$  in the limit  $\mu \rightarrow 0^+$  has a fixed point with stability multiplier  $-1$  when  $r = r_0 \approx 0.66691$ . Moreover, the assumptions of theorem 3 hold using  $\eta = \sigma - \sigma_0$  for the second parameter. Thus for  $\mu > 0$  period-doubling bifurcations occur on a curve  $\sigma = \sigma_0 + g(\mu)$  with  $g(0) = 0$ . We computed this curve numerically and it is shown in Figure 6a. By eq. (26) the curve emanates from the codimension-two point  $(\mu, \sigma) = (0, \sigma_0)$  with slope  $-\frac{ac+d}{bc+e}$ . For this example  $a \approx 2.6886$ ,  $b \approx -2.0195$ ,  $c \approx 1.0021$ ,  $d \approx 0.9756$ , and  $e \approx -5.2383$  (also  $f \approx 0.6332$ ). In Figure 6a we show the line through  $(\mu, \sigma) = (0, \sigma_0)$  with slope  $-\frac{ac+d}{bc+e}$  as a dashed line, and indeed this appears to match the slope of our numerically computed period-doubling bifurcation curve. ( $\mu = 0$ ,  $\eta = 0$ )

The BEB and period-doubling bifurcation curves divide the parameter plane locally into three regions. For  $\mu < 0$  the system has an unstable pseudo-equilibrium, while for  $\mu > 0$  it has an unstable regular equilibrium and a single-impact limit cycle. Below the period-doubling curve this limit cycle is stable, whereas immediately above the period-doubling curve it is unstable and there is a stable two-impact limit cycle. Further above the period-doubling curve stable multi-impact limit cycles exist due to the occurrence of a period-doubling cascade, described below.

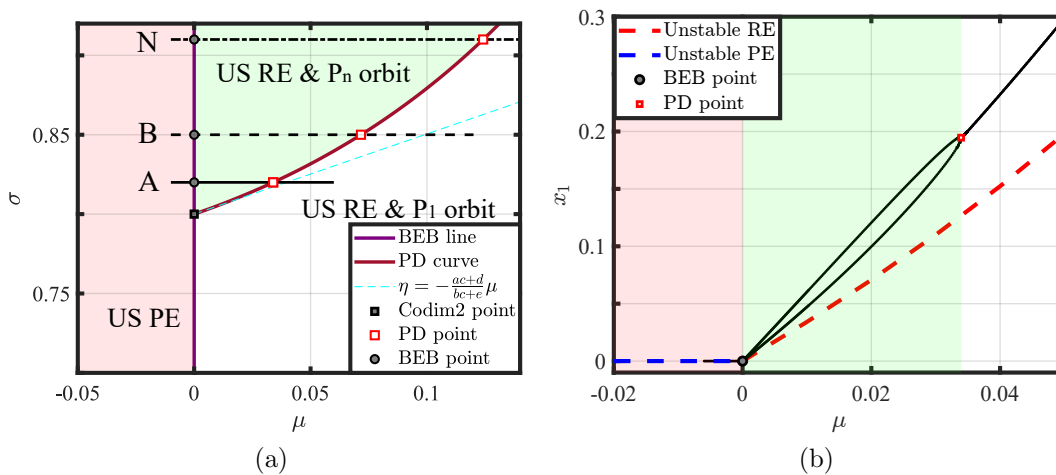


Figure 6: (a) A two-parameter bifurcation diagram for Example 4.3 with  $r = r_0 \approx 0.66691$  as discussed in the text. (b) A one-parameter bifurcation diagram using also  $\sigma = 0.82$ . This corresponds to the line  $A$  shown in panel (a); slices along the lines  $B$  and  $N$  are shown in Figure 8.

Next we describe several bifurcation diagrams defined by fixing  $\sigma > \sigma_0$ . First Figure 6b uses  $\sigma = 0.82$  (i.e.  $\eta = 0.02$ ). This shows a stable two-impact limit cycle

being created in the BEB at  $\mu = 0$ , and coexisting with the regular equilibrium. The limit cycle exists up until the period-doubling bifurcation at  $\mu_{\text{PD}} = \eta^{-1}(\sigma - \sigma_0) \approx 0.033941$  beyond which there is a stable single-impact limit cycle.

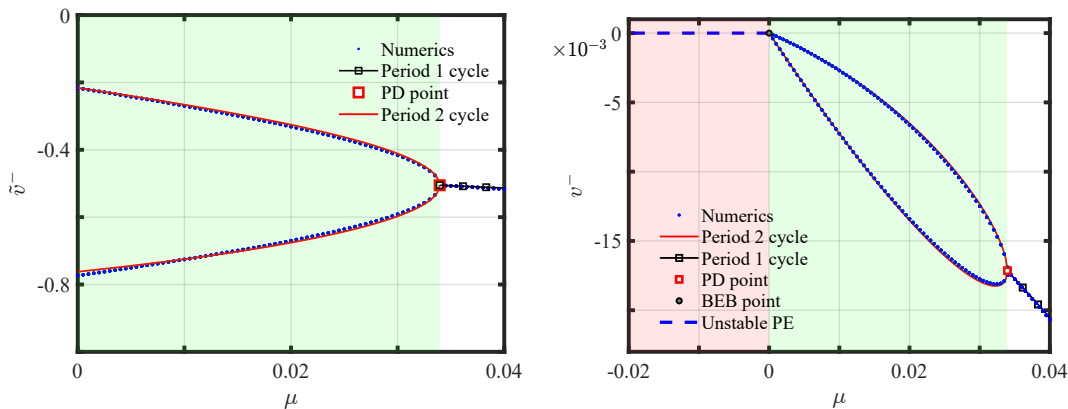


Figure 7: The impact velocities of the single-impact and two-impact limit cycles of Figure 6b in blown-up co-ordinates (panel (a)), and original co-ordinates (panel (b)). The blue points are the numerically obtained impact velocities, while the curves are the theoretical approximations (31) and (32). Similar to Figure 4 but showing the agreement between theory and numerics for the BEB-PD case in example 4.3.

As shown in appendix B, the impact velocity in blown-up co-ordinates of the single-impact limit cycle is well approximated by

$$\hat{A} = \ell_0 + \ell_1\mu + L_{01}\frac{a(\mu - \mu_{\text{PD}})}{2}, \quad (31)$$

where  $\ell_0 \approx -0.5053$ ,  $\ell_1 = 0$ , and  $L_{01} \approx -0.9899$  for this example. Furthermore

$$\text{give } \hat{A} = \ell_0 + \ell_1\mu + L_{01} \left( \pm \sqrt{-\frac{(ca + d)(\mu - \mu_{\text{PD}})}{c^2 + f}} + \frac{c(ca + d)}{2(c^2 + f)}(\mu - \mu_{\text{PD}}) + \frac{a(\mu - \mu_{\text{PD}})}{2} \right) \quad (32)$$

approximates the two impact velocities of the two-impact limit cycle. As shown in Figure 7a these provide excellent agreement to the numerically computed values, and Figure 7b shows these in the original unscaled co-ordinates.

Next, the left column of Figure 8 uses  $\sigma = 0.85$ , corresponding to slice B in Figure 6a. Specifically Figure 8a uses original co-ordinates and Figure 8c uses blown-up co-ordinates. As we move right to left across either plot, the single-impact limit cycle

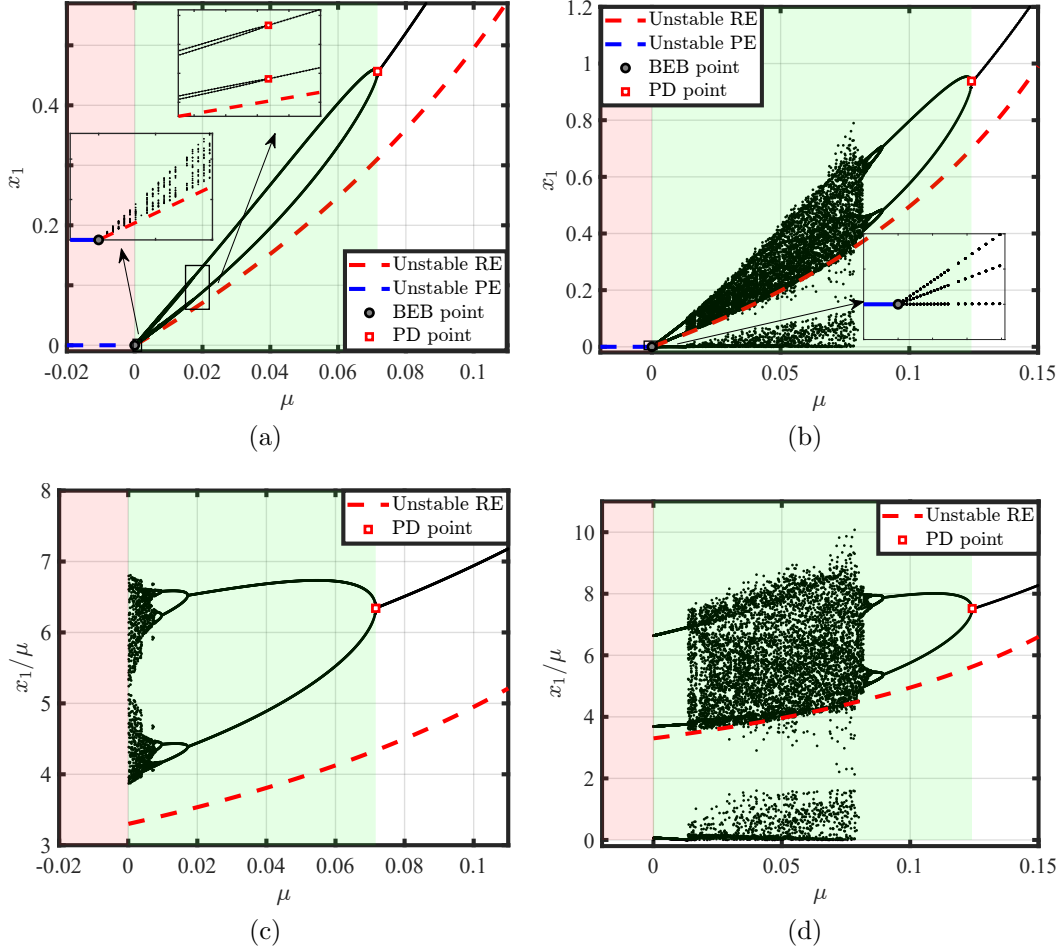


Figure 8: Bifurcation diagrams for Example 4.3 with  $r = r_0 \approx 0.66691$ . Panels (a) and (c) use  $\sigma = 0.85$  corresponding to slice B in Figure 6a, while panels (b) and (d) use  $\sigma = 0.91$  corresponding to slice N. The top panels use original co-ordinates, while the bottom panels use blown-up co-ordinates.

loses stability in a period-doubling bifurcation, as in Figure 6b, but now this appears to be followed by a full period-doubling cascade resulting in a chaotic attractor. As we instead move left to right, this attractor is born in the BEB at  $\mu = 0$ . This suggests that as we increase the value of  $\sigma$  from 0.82 to 0.85, we pass through infinitely many period-doubling bifurcation curves. We expect each of these emanates transversally from the BEB curve at some  $0.82 < \sigma < 0.85$ , and this could be verified formally by applying theorem 3 to higher iterates of  $P$ .

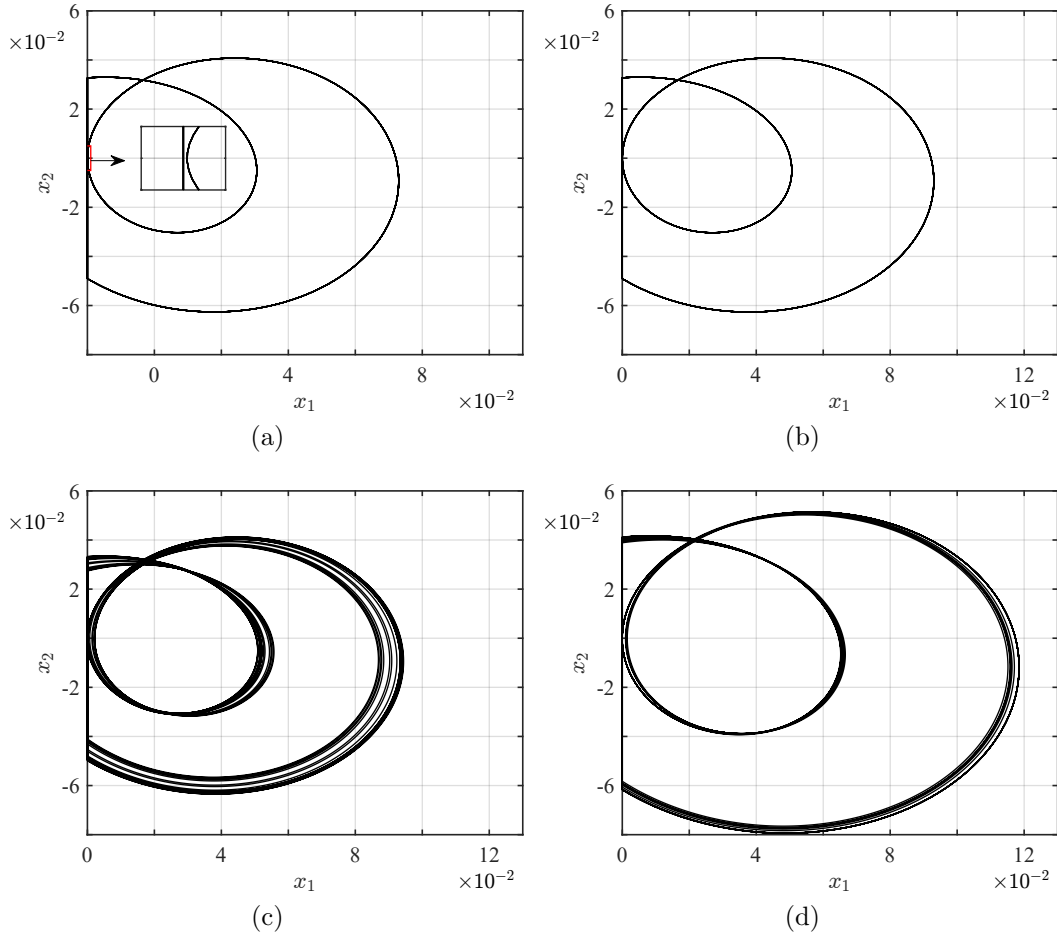


Figure 9: Phase portraits showing the attractor of Example 4.3 with  $r = r_0 \approx 0.66691$ ,  $\sigma = 0.91$ , and four different values of  $\mu$ : (a)  $\mu = 0.01345$ ; (b)  $\mu = 0.0134597$ ; (c)  $\mu = 0.01355$ ; (d)  $\mu = 0.017$ . As the value of  $\mu$  is increased, a stable limit cycle undergoes a grazing bifurcation at  $\mu \approx 0.0134597$  and appears to be replaced by a chaotic attractor.

Finally, the right column of Figure 8 uses  $\sigma = 0.91$ , corresponding to slice N in Figure 6a. Now the BEB creates a stable period-two limit cycle. At  $\mu \approx 0.0134597$  the limit cycle appears to be converted to a chaotic attractor through a grazing bifurcation (i.e. zero velocity impacts), see Figure 9. The chaotic attractor appears to extend until  $\mu \approx 0.075$  where it undergoes a kind of boundary crisis caused by grazing behaviour of the chaotic attractor. A different kind of chaotic attractor now

occurs, and this is subsequently destroyed in a reverse period-doubling cascade.

**Example 4.4.** *Suppose the coefficients are as in All the parameters are the same as in example 4.3, except*

$$(a). \quad q_1 = -1, \quad q_2 = 0 ; \quad (b). \quad q_1 = 0, \quad q_2 = -1 ;$$

and we allow various values of  $\epsilon \geq 0$ .

■

We now consider  $\epsilon \neq 0$  to investigate the effect of nonlinear terms. We return to slice A of Figure 6b where a stable two-impact limit cycle is created at the BEB, and this occurs for any value of  $\epsilon$ . Different values of  $\epsilon$  affect the dynamics and bifurcations occurring for  $\mu > 0$ , see Figure 10. With  $\epsilon = 0.1$  the bifurcation structure is qualitatively unchanged in that the two-impact limit cycle reverts to a single-impact limit cycle in a (reverse) period-doubling bifurcation, but for larger values of  $\epsilon$  the attractor appears to be chaotic in some places.

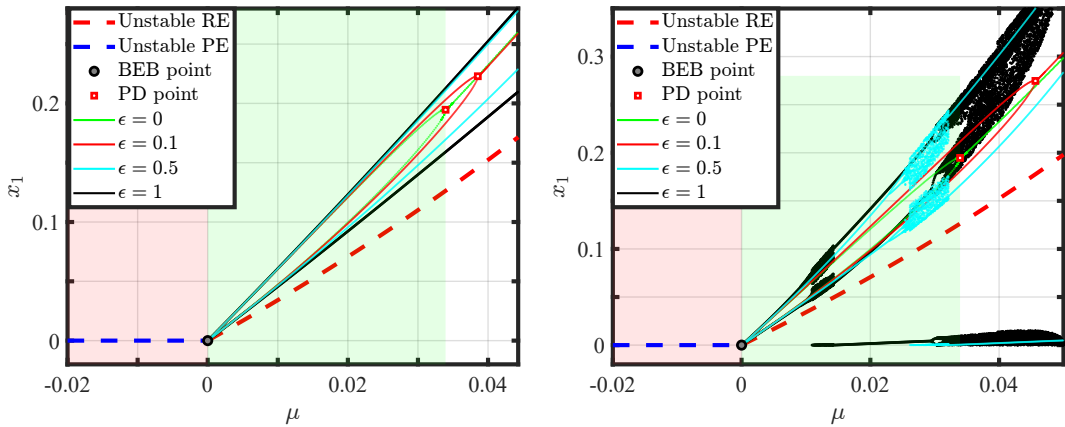


Figure 10: One-parameter bifurcation diagrams for example 4.4 with  $r = r_0 \approx 0.66691$ ,  $\sigma = 0.82$ , and various values of  $\epsilon$ . Panel (a) uses  $q_1 = -1$  and  $q_2 = 0$ , while panel (b) uses  $q_1 = 0$  and  $q_2 = -1$ .

### 4.3 An eight-dimensional wing-flap model

Here we replicate numerical results from [40] for a simplified airfoil model illustrated in Figure 11. Due to rotary freeplay in the hinge between the flap and main body,



the system is well modelled as an impacting hybrid system, where a reset map is applied when the flap hits the stop. Using Lagrangian mechanics and approximated aerodynamics, see details in [39], the governing equations of motion can be written as

$$\begin{cases} \dot{\mathbf{x}} = \mathbf{A}_{\text{af}}(\bar{U})\mathbf{x} + \mathbf{G}(\bar{U}), & \text{for } |\beta| < \delta, \\ \mathbf{x} = R(\mathbf{x}), & \text{for } |\beta| = \delta, \end{cases} \quad (33)$$

where  $\mathbf{x} = [\zeta, \alpha, \beta, \dot{\zeta}, \dot{\alpha}, \dot{\beta}, w_1, w_2]^\top$ . Here  $\alpha$  is the rotary pitch,  $\beta$  is the flap position,  $\zeta$  is the dimensionless heave, and  $w_1$  and  $w_2$  are augmented variables that capture Theodorsen aerodynamic interactions [41]. The parameter  $\bar{U}$  is the dimensionless air velocity over linear flutter velocity  $U_f = 30$  m/s, and  $\delta$  characterizes the amount of flap freeplay. The matrix  $\mathbf{A}_{\text{af}}$  specifies the dynamics of the airfoil when the flap is in freeplay. The reset map  $R(\mathbf{x})$  is affine and models impacts with a coefficient of restitution  $0 < r < 1$  in the sense that  $\dot{\beta} \mapsto -r\dot{\beta}$ . Full details of the model including the coefficients of  $\mathbf{A}_{\text{af}}$  and  $\mathbf{G}$  are given in Appendix C.

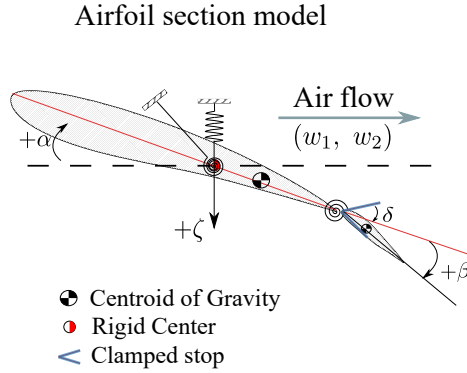


Figure 11: A sketch illustrating the variables of the airfoil model (33).

Figure 12, taken from [39], shows a typical bifurcation diagram of the airfoil model. We use the flow velocity  $\bar{U}$  as the bifurcation parameter, while the remaining parameters are fixed at

$$\delta = 0.01, \quad r = 0.72, \quad \xi_h = \xi_\alpha = \xi_\beta = 0.02. \quad (34)$$

Specifically, we see a stable regular equilibrium collides with the impacting surface  $\beta = -\delta$  at  $\bar{U} \approx 0.64833$ , beyond which the system has a stable pseudo-equilibrium coexisting with a stable single-impact limit cycle. The limit cycle subsequently undergoes smooth bifurcations near the impacting surface, and this is what motivates our studies of codimension-two BEBs.

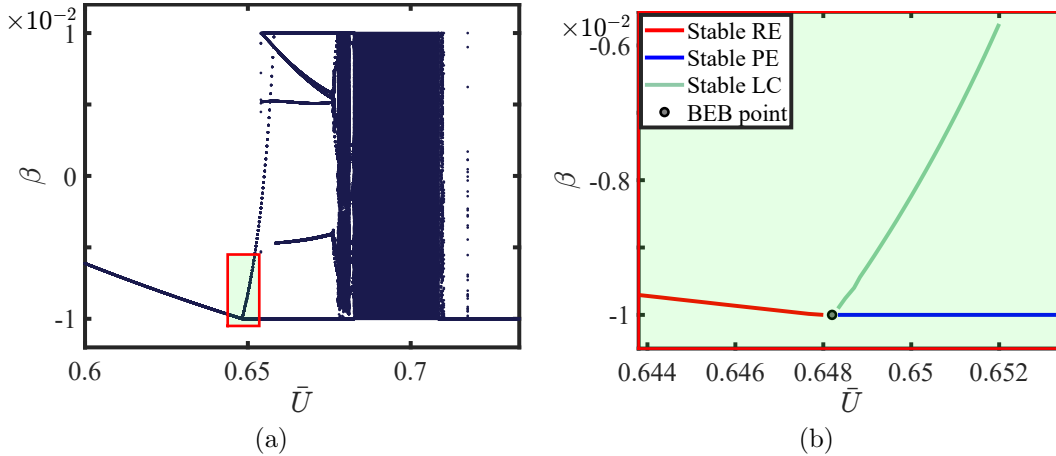


Figure 12: Brute force bifurcation diagram of the airfoil model eq. (33); (a) the full bifurcation diagram capturing various dynamics, (b) zoomed-in part of the first bifurcation from boxed region in (a): *PE* – Pseudo Equilibria, *RE* – Regular Equilibria. Full equations and parameter definitions are given in appendix C.

#### 4.3.1 BEB-saddle-node bifurcation

Using the algorithm and continuation techniques of [39], we tracked a curve of saddle-node bifurcations of single-impact limit cycles in the  $(\bar{U}, r)$  parameter plane, Figure 13a. We found this curve meets the BEB at the codimension-two point  $(\bar{U}_0, r_0) \approx (0.64833, 0.6292)$ . Here the normal form (20) has coefficients

$$a \approx 5.1754, \quad b \approx 44.1124,$$

and in agreement with (22) the saddle-node bifurcation curve appears to have slope  $-\frac{a}{b}$  at the codimension-two point.

Figure 13b shows a typical one-parameter bifurcation diagram containing both the BEB and saddle-node bifurcations. At the BEB the stable state changes from a regular equilibrium to a pseudo-equilibrium, while at the saddle-node bifurcation stable and unstable limit cycles are born (only the stable limit cycle is indicated in the figure as it was computed numerically via direct integration of (33)). Note that since the one-parameter bifurcation diagram corresponds to a slice below the codimension-two point where no limit cycles are created in the BEB, bifurcation diagram shows a different sequence of dynamics to Figure 3b.

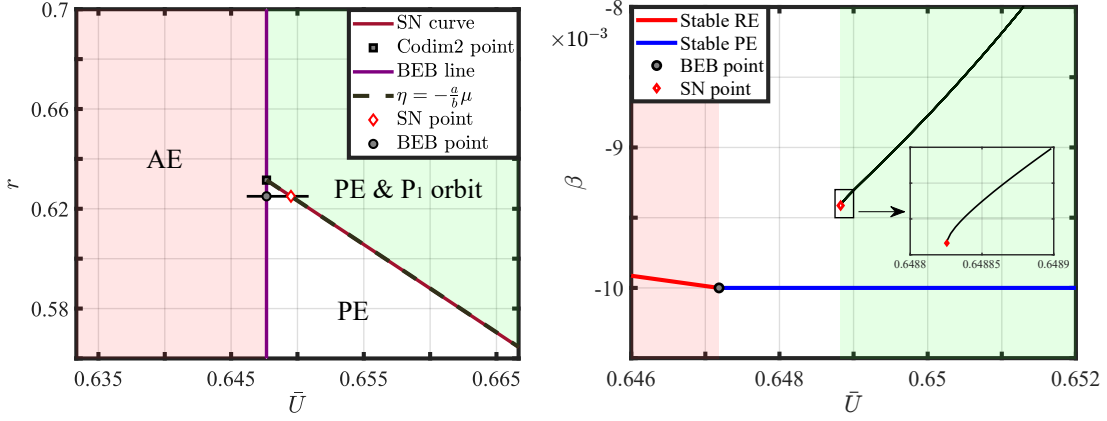


Figure 13: (a) A two-parameter bifurcation diagram showing the unfolding of a BEB-saddle-node bifurcation in the airfoil model (33) with  $\delta = 0.01$  and  $\xi_h = \xi_\alpha = \xi_\beta = 0.02$ . (b) A one-parameter bifurcation diagram corresponding to setting also  $r = 0.625$ .

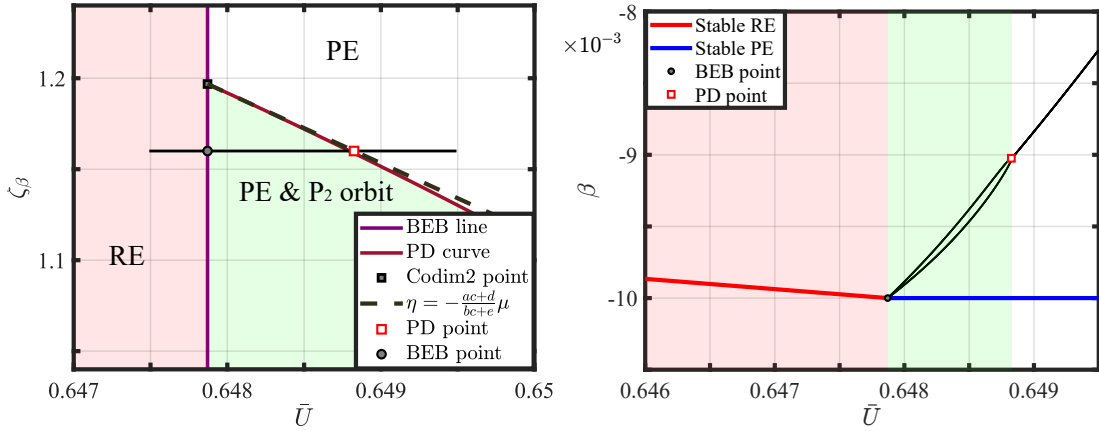


Figure 14: (a) A two-parameter bifurcation diagram showing the unfolding of a BEB-period-doubling bifurcation of the airfoil model (33) with  $\delta = 0.01$ ,  $r = 0.72$ , and  $\xi_h = \xi_\alpha = 0.02$ . (b) A one-parameter bifurcation diagram corresponding to setting also  $\xi_\beta = 0.0116$ .

### 4.3.2 BEB-period-doubling bifurcation

By now fixing  $r = 0.72$  and varying  $\bar{U}$  and  $\xi_\beta$ , we found that a curve of period-doubling bifurcations of single-impact limit cycles meets the BEB at  $(\bar{U}_0, \xi_\beta^0) \approx$

(0.64833, 0.011793), see Figure 14a. Here the normal form (25) has coefficients

$$a \approx 16.0757, \quad b \approx -3.5337, \quad c \approx 0.0046, \quad d \approx 0.0595, \quad e \approx 0.2627,$$

and as expected, the period-doubling curve appears to have slope  $-\frac{ac+d}{bc+e}$  at the codimension-two point.

Figure 14b shows a nearby one-parameter bifurcation diagram. The BEB creates a stable two-impact limit cycle that reverts to a single-impact limit cycle in the period-doubling bifurcation.

## 5 Discussion

In this paper two codimension-two boundary equilibrium bifurcations (BEBs) have been analysed for the first time. These are situations where the number and nature of the small-amplitude limit cycles born at BEBs vary due to saddle-node or period-doubling bifurcations of limit cycles. Analogous situations involving a Neimark-Sacker bifurcation are left for future work.

Future work should also consider global bifurcations of the small-amplitude limit cycles that emerge from a BEB; see for example the case of a homoclinic boundary focus identified in [8], and forthcoming work [30] featuring the local birth of Shilnikov-grazing dynamics.

Clearly there are many more behaviours that can be born locally from a BEB, including, as illustrated in fig. 8, two different kinds of chaotic attractors. A detailed study of the local creation of chaotic attractors is beyond the scope of the present study, and it would be particularly interesting to see how these arise beyond a cascade of codimension-two BEB-period-doubling bifurcations. We expect that the codimension-two BEBs admit the same types of unfoldings for Filippov systems and piecewise-smooth continuous ODEs because in each case the blown-up system is piecewise-linear in the limit  $\mu \rightarrow 0^+$ .

## Acknowledgments

Hong Tang was supported by the University of Bristol & China Scholarship Council joint studentship, No.202006120007. David Simpson was supported by Marsden Fund contract MAU2209 managed by Royal Society Te Apārangi. The authors thank Mike Jeffrey for helpful conversations.

## References

- [1] V.I. Arnold. *Ordinary Differential Equations*. MIT press, 1973.
- [2] M. di Bernardo, C.J. Budd, and A.R. Champneys. “Normal form maps for grazing bifurcations in  $n$ -dimensional piecewise-smooth dynamical systems.” In: *Phys. D* 160 (2001), pp. 222–254.
- [3] M. di Bernardo, A Nordmark, and G Olivar. “Discontinuity-induced bifurcations of equilibria in piecewise-smooth and impacting dynamical systems”. In: *Physica D: Nonlinear Phenomena* 237.1 (2008), pp. 119–136. ISSN: 01672789. DOI: 10.1016/j.physd.2007.08.008. URL: [www.elsevier.com/locate/physd](http://www.elsevier.com/locate/physd).
- [4] M. di Bernardo, D.J. Pagano, and E. Ponce. “Nonhyperbolic boundary equilibrium bifurcations in planar Filippov systems: A case study approach.” In: *Int. J. Bifurcation Chaos* 18.5 (2008), pp. 1377–1392.
- [5] B. Brogliato. *Nonsmooth Mechanics: Models, Dynamics and Control*. third. Springer International Publishing, 2016. ISBN: 9783319286648. URL: <http://dx.doi.org/10.1007/978-3-319-28664-8>.
- [6] T. Carvalho, D.D. Novaes, and L.F. Gonçalves. “Sliding Shilnikov connection in Filippov-type predator-prey model.” In: *Nonlinear Dyn.* 100 (2020), pp. 2973–2987.
- [7] F. Della Rossa and F. Dercole. “Generalized boundary equilibria in  $n$ -dimensional Filippov systems: The transition between persistence and nonsmooth-fold scenarios.” In: *Phys. D* 241 (2012), pp. 1903–1910.
- [8] F. Dercole et al. “Two Degenerate Boundary Equilibrium Bifurcations in Planar Filippov Systems”. In: *SIAM Journal on Applied Dynamical Systems* 10.4 (Jan. 2011), 1525–1553. ISSN: 1536-0040. URL: <http://dx.doi.org/10.1137/100812549>.
- [9] M. di Bernardo et al. *Piecewise-smooth dynamical systems: theory and applications*. English. Applied Mathematical Sciences. Springer, Jan. 2008. ISBN: 9781846280399. DOI: 10.1007/978-1-84628-708-4.
- [10] M.I. Feigin. “On the structure of C-bifurcation boundaries of piecewise-continuous systems”. In: *Journal of Applied Mathematics and Mechanics* 42.5 (Jan. 1978), 885–895. DOI: 10.1016/0021-8928(78)90035-7. URL: [http://dx.doi.org/10.1016/0021-8928\(78\)90035-7](http://dx.doi.org/10.1016/0021-8928(78)90035-7).

- [11] A. F. Filippov. *Differential Equations with Discontinuous Righthand Sides*. Ed. by F. M. Arscott. Springer Netherlands, 1988. ISBN: 9789401577939. DOI: 10.1007/978-94-015-7793-9.
- [12] M.H. Fredriksson and A.B. Nordmark. “Bifurcations caused by grazing incidence in many degrees of freedom impact oscillators.” In: *Proc. R. Soc. A* 453 (1997), pp. 1261–1276.
- [13] M.H. Fredriksson and A.B. Nordmark. “On normal form calculation in impact oscillators.” In: *Proc. R. Soc. A* 456 (2000), pp. 315–329.
- [14] E. Freire et al. “Bifurcation Sets of Continuous Piecewise Linear Systems with Two Zones.” In: *Int. J. Bifurcation Chaos* 8.11 (1998), pp. 2073–2097.
- [15] P. Glendinning. “Classification of Boundary Equilibrium Bifurcations in planar Filippov systems.” In: *Chaos* 26 (2016), p. 013108.
- [16] P. Glendinning and M.R. Jeffrey. “Grazing-sliding bifurcations, border collision maps and the curse of dimensionality for piecewise smooth bifurcation theory.” In: *Nonlinearity* 28 (2015), pp. 263–283.
- [17] P.A. Glendinning. “Shilnikov chaos, Filippov sliding and Boundary Equilibrium Bifurcations.” In: *Euro. J. Appl. Math.* 29 (2018), pp. 757–777.
- [18] R. Goebel, R.G. Sanfelice, and A.R. Teel. *Hybrid Dynamical Systems: Modeling, Stability, and Robustness*. Princeton University Press, Mar. 2012. ISBN: 9781400842636.
- [19] M. Guardia, T.M. Seara, and M.A. Teixeira. “Generic bifurcations of low codimension of planar Filippov Systems.” In: *J. Diff. Eq* 250 (2011), pp. 1967–2023.
- [20] J. Guckenheimer and P. Holmes. *Nonlinear Oscillations, Dynamical Systems, and Bifurcations of Vector Fields*. Applied mathematical sciences. Springer-Verlag, 1983. ISBN: 9780387908199. URL: <https://books.google.co.uk/books?id=OLg-AQAAIAAJ>.
- [21] W.M. Haddad, V. Chellaboina, and S.G. Nersesov. *Impulsive and Hybrid Dynamical Systems. Stability, Dissipativity, and Control*. Princeton, NJ: Princeton University Press, 2006.
- [22] S.J. Hogan et al. “Piecewise smooth dynamical systems theory: the case of the missing boundary equilibrium bifurcations.” In: *J. Nonlin. Sci.* 26 (2016), pp. 1161–1173.

- [23] A.P. Ivanov. “Stability of Periodic Motions with Impacts.” In: *Impacts in Mechanical Systems: Analysis and Modelling*. Ed. by B. Brogliato. New York: Springer-Verlag, 2000.
- [24] M.R. Jeffrey. *Hidden Dynamics. The Mathematics of Switches, Decisions and Other Discontinuous Behaviour*. New York: Springer, 2018.
- [25] K.H. Johansson et al. “On the regularization of Zeno hybrid automata.” In: *Systems and Control Letters* 38 (1999), pp. 141–150.
- [26] R. T Jones. *Operational treatment of the non-uniform lift theory in airplane dynamics*. 1938. URL: <https://digital.library.unt.edu/ark:/67531/metadc54463/>.
- [27] Yu.A. Kuznetsov, S. Rinaldi, and A. Gragnani. “One-Parameter Bifurcations in Planar Filippov Systems.” In: *Int. J. Bifurcation Chaos* 13.8 (2003), pp. 2157–2188.
- [28] Yuri A. Kuznetsov. *Elements of applied bifurcation theory*. 2nd ed. Applied Mathematical Sciences 112. Berlin: Springer, 1998. ISBN: 978-0387983820.
- [29] A.B. Nordmark. “Non-periodic motion caused by grazing incidence in impact oscillators.” In: *J. Sound Vib.* 2 (1991), pp. 279–297.
- [30] A.B. Nordmark et al. *Dynamics near a grazing Shilnikov homoclinic orbit in impacting systems*. In preparation. 2024.
- [31] D.D. Novaes and M.A. Teixeira. “Shilnikov Problem in Filippov Dynamical Systems.” In: *Chaos* 29 (2019), p. 063110.
- [32] A.J. Van der Schaft and J.M. Schumacher. *An Introduction to Hybrid Dynamical Systems*. New York: Springer-Verlag, 2000.
- [33] D. J. W. Simpson. “A general framework for boundary equilibrium bifurcations of Filippov systems”. In: *Chaos* 28.10 (Oct. 2018). ISSN: 1089-7682. URL: <http://dx.doi.org/10.1063/1.5037947>.
- [34] D.J.W. Simpson. *Bifurcations in Piecewise-Smooth Continuous Systems*. Vol. 70. Nonlinear Science. Singapore: World Scientific, 2010.
- [35] D.J.W. Simpson. “The instantaneous local transition of a stable equilibrium to a chaotic attractor in piecewise-smooth systems of differential equations”. In: *Physics Letters A* 380.38 (2016), pp. 3067–3072. ISSN: 0375-9601. DOI: <https://doi.org/10.1016/j.physleta.2016.07.033>.
- [36] D.J.W. Simpson. “Twenty Hopf-like bifurcations in piecewise-smooth dynamical systems.” In: *Phys. Rep.* 970 (2022), pp. 1–80.

- [37] D.J.W. Simpson, D.S. Kompala, and J.D. Meiss. “Discontinuity Induced Bifurcations in a Model of *Saccharomyces cerevisiae*.” In: *Math. Biosci.* 218.1 (2009), pp. 40–49.
- [38] D.J.W. Simpson and J.D. Meiss. “Aspects of bifurcation theory for piecewise-smooth, continuous systems”. In: *Physica D: Nonlinear Phenomena* 241.22 (2012), pp. 1861–1868. ISSN: 0167-2789. DOI: <https://doi.org/10.1016/j.physd.2011.05.002>. URL: <https://www.sciencedirect.com/science/article/pii/S0167278911001096>.
- [39] H. Tang and A.R. Champneys. “Bifurcation of Limit Cycles from Boundary Equilibria in Impacting Hybrid Systems”. In: *SIAM Journal on Applied Dynamical Systems* 22.4 (2023), pp. 3320–3357. DOI: 10.1137/23M1552292. URL: <https://doi.org/10.1137/23M1552292>.
- [40] H. Tang, A.R. Champneys, and N. Lieven. *Bifurcation analysis of an airfoil model with freeplay*. In preparation. 2024.
- [41] T. Theodorsen. “General theory of aerodynamic instability and the mechanism of flutter”. In: *Journal of the Franklin Institute* 219.6 (1935), pp. 766–767. ISSN: 00160032. DOI: 10.1016/S0016-0032(35)92022-1.
- [42] M. Wiercigroch and B. De Kraker, eds. *Applied Nonlinear Dynamics and Chaos of Mechanical Systems with Discontinuities*. Singapore: World Scientific, 2000.
- [43] J.R. Wright and J.E. Cooper. *Introduction to Aircraft Aeroelasticity and Loads*. Aerospace Series. Wiley, 2008. ISBN: 9780470858462.
- [44] J. Zhang et al. “Zeno hybrid systems.” In: *Int. J. Robust Nonlinear Control* 11 (2001), pp. 435–451.



# A Numerical computation of the restricted map

## A.1 Parameter-dependent fixed point problem

Let us start by extending the results in [28] to consider the parameter dependence of the normal form of saddle-node and period-doubling bifurcations more explicitly. Consider a map

$$x \mapsto P(x; \alpha)$$

where  $x \in \mathbb{R}^n$  and  $\alpha \in \mathbb{R}$ . We will derive formulas for the first few terms of the restriction of  $P$  to a centre manifold associated with a saddle-node or period-doubling bifurcation.

Suppose  $P(0; 0) = 0$ , so that the origin  $x = 0$  is a fixed point of  $P$  when  $\alpha = 0$ , and write

$$P(x; \alpha) = \alpha\gamma + A(\alpha)x + F(x; \alpha), \quad (35)$$

where  $\gamma = \frac{\partial P}{\partial \alpha}$  is an  $n$ -dimensional constant vector,  $A(\alpha) \in \mathbb{R}^{n \times n}$ , and  $F$  contains all other terms.

At  $\alpha = 0$ , let us suppose that there is a unique multiplier  $\lambda_0$  of  $A(0)$  such that  $|\lambda_0| = 1$  ( $\lambda_0 = 1$  for the saddle node case and  $\lambda_0 = -1$  for period doubling). Let  $\lambda(\alpha)$  be a continuous family of such multipliers, and choose  $w(\alpha)$  and  $v(\alpha)$  to be smooth families of the corresponding left and right eigenvectors, respectively, normalized so that  $w^\top v = 1$  for all small  $\alpha$ . Henceforth we shall use a subscript 0 for any variable calculated at  $\alpha = 0$  and otherwise drop dependence on  $\alpha$  whenever the meaning is clear. Thus,  $\lambda = w^\top A v$  for all small  $\alpha$ .

Then we make the  $\alpha$ -dependent projection of  $x$  into components in the kernel and range of  $(A - \lambda I)$  via

$$x = zv + y, \quad \text{where } z = w^\top x, \quad y = x - w^\top x,$$

and write the map  $P$  in the new co-ordinates as coordinates

$$\begin{aligned} z &\mapsto \tilde{z} := \nu\alpha + \lambda z + w^\top F(zv + y; \alpha) \\ y &\mapsto \tilde{y} := \kappa\alpha + Ay + F(zv + y; \alpha) - w^\top F(zv + y; \alpha)v \end{aligned} \quad (36)$$

where  $\nu = w^\top \gamma$  is a scalar and  $\kappa = \gamma - w^\top \gamma v \in \mathbb{R}^n$ .

We now follow the projection method of Kuznetsov [28, pg. 174] to obtain the normal form. We start by writing the nonlinear part using the multivariable Taylor expansion,

$$F = \frac{1}{2}B(x, x) + \frac{1}{6}C(x, x, x) + \text{H.O.T.},$$

where  $B$  is a third-order and  $C$  a fourth-order tensor (these are unrelated to the matrices  $B$  and  $C$  used in the main body of the paper). Then we can write eq. (36) in the form

$$\begin{aligned}\tilde{z} &= \nu\alpha + \lambda z + cz^2 + w^\top B(v, y)z + rz^3 + \text{H.O.T.} \\ \tilde{y} &= \kappa\alpha + Ay + \frac{1}{2}H_{02}z^2 + B(v, y)z - zw^\top B(v, y)v + \frac{1}{2}B(y, y) - \frac{1}{2}w^\top B(y, y)v + \text{H.O.T.},\end{aligned}\tag{37}$$

where

$$c = \frac{1}{2}w^\top B(v, v), \quad r = \frac{1}{6}w^\top C(v, v, v), \quad H_{02} = B(v, v) - w^\top B(v, v)v.$$

Next, let us suppose we write the center manifold of eq. (37) as

$$y = V(z, \alpha) := w_{01}\alpha + w_{11}\alpha z + \frac{1}{2}w_{20}z^2 + \frac{1}{2}w_{02}\alpha^2 + \text{H.O.T.},\tag{38}$$

where the  $w_{ij}$  are vectors that we need to calculate. We then substitute eq. (38) into eq. (37), in order to write the restricted map as

$$\tilde{z} = \nu\alpha + \lambda(\alpha)z + cz^2 + w^\top B(v, w_{01})\alpha z + \left(\frac{1}{2}w^\top B(v, w_{20}) + r\right)z^3 + \text{H.O.T.}\tag{39}$$

Similarly, for the  $y$  component we obtain

$$\begin{aligned}\tilde{y} &= \kappa\alpha + Aw_{01}\alpha + Aw_{11}\alpha z + \frac{1}{2}Aw_{20}z^2 + \frac{1}{2}H_{02}z^2 \\ &+ (B(v, w_{01}) - w^\top B(v, w_{01})v)\alpha z + \frac{1}{2}B(y, y) - \frac{1}{2}w^\top B(y, y)v + \text{H.O.T.}\end{aligned}\tag{40}$$

In order to obtain the unknown coefficient vectors  $w_{01}, w_{11}, w_{20}$ , we have to solve the homological equation

$$\tilde{y} = V(\tilde{z}, \tilde{\alpha})\tag{41}$$

After, substituting the expression eq. (39) for  $\tilde{z}$  into  $V$  defined by eq. (38), we find the first few terms of the right-hand side of eq. (41) are

$$V(\tilde{z}, \alpha) = w_{01}\alpha + w_{11}\alpha(\nu\alpha + \lambda(\alpha)z) + \frac{1}{2}w_{20}(\nu\alpha + \lambda(\alpha)z + \dots)^2 + \text{H.O.T.},$$

We now solve eq. (41) term by term, by matching coefficients of  $\alpha, \alpha z$  and  $z^2$ . From this we obtain

$$\kappa + Aw_{01} = w_{01}\tag{42}$$

$$Aw_{11} + B(v, w_{01}) - w^\top B(v, w_{01})v = w_{11}\lambda_0 + w_{20}\nu\lambda_0\tag{43}$$

$$Aw_{20} + H_{02} = w_{20}.\tag{44}$$

Looking at the first equation, note that in the case of the saddle-node, the definition of  $\kappa$  ensures that it is in the range of  $(A - I)$ , therefore we can find a solution up to a scalar constant. The same is true for all the  $w_{ij}$ , for both the saddle-node and period-doubling cases. In particular, we find

**SN case:**  $\lambda_0 = 1$ .

$$\begin{aligned} w_{01} &= (I - A)^{\text{INV}}(\gamma - w^\top \gamma v), \\ w_{11} &= (I - A)^{\text{INV}}[B(v, w_{01}) - w^\top B(v, w_{01})v - w_{20}v], \\ w_{20} &= (I - A)^{\text{INV}}H_{02}; \end{aligned}$$

**PD case:**  $\lambda_0 = -1$ .

$$\begin{aligned} w_{01} &= (I - A)^{-1}(\gamma - w^\top \gamma v) = (I - A)^{-1}\gamma - \frac{w^\top \gamma}{2}w, \\ w_{11} &= -(I + A)^{\text{INV}}[B(v, w_{01}) - w^\top B(v, w_{01})v + w_{20}v], \\ w_{20} &= (I - A)^{-1}H_{02}. \end{aligned}$$

Here INV represents a pseudo-inverse computation, which is needed when the matrix is not invertible, but the right-hand side is in the range of the operator. In that case, the solution is only defined up to a scalar (see [28, pg. 184] for details).

It is helpful in what follows to notice that

$$\frac{\partial^2 \tilde{z}}{\partial \alpha \partial z} = w^\top D \frac{\partial P}{\partial \alpha} v + w^\top B(v, w_{01}).$$

## A.2 Evaluation of coefficients of restricted maps

We now show how the above results enable us to find closed form expressions for all the coefficients in (20) and (25) in terms of the (full) Poincaré map  $P(u; \mu, \eta)$  and its derivatives. In particular, following the logic of the previous section, with  $\alpha$  replaced by either  $\mu$  or  $\eta$ , we find the coefficients of (20) and (25) are given by

$$a = w^\top \frac{\partial P}{\partial \mu}, \quad b = w^\top \frac{\partial P}{\partial \eta}, \quad c = \frac{1}{2} w^\top [(D^2 P)(v, v)];$$

with

$$d = w^\top D \frac{\partial P}{\partial \mu} v + w^\top B(v, (I - A)^{\text{INV}}(\frac{\partial P}{\partial \mu} - av)), \quad e = w^\top D \frac{\partial P}{\partial \eta} v + w^\top B(v, (I - A)^{\text{INV}}(\frac{\partial P}{\partial \eta} - bv)),$$

$$m = \frac{1}{2}w^\top \frac{\partial^2 P}{\partial \mu^2}, \quad n = \frac{1}{2}w^\top \frac{\partial^2 P}{\partial \eta^2}, \quad f = \frac{1}{6}w^\top C(v, v, v) + \frac{1}{2}w^\top B(w, B(w, (I-A)^{\text{INV}} H_{02}));$$

in the saddle-node case, and

$$d = w^\top D \frac{\partial P}{\partial \mu} v + w^\top B(v, (I-A)^{-1}(\frac{\partial P}{\partial \mu} - av)), \quad e = w^\top D \frac{\partial P}{\partial \eta} v + w^\top B(v, (I-A)^{-1}(\frac{\partial P}{\partial \eta} - bv)),$$

$$f = \frac{1}{6}w^\top C(v, v, v) - c^2 + \frac{1}{2}w^\top B(w, B(w, (I-A)^{-1}B(v, v))).$$

in the period-doubling case.

## B Approximation of the bifurcating limit cycles

Here, we provide approximate expressions for the amplitudes of the bifurcating limit cycles. We use the incoming (impact) velocities of the limit cycles to measure their amplitude. These are obtained by evaluating the velocity relative to the impacting surface at the corresponding fixed points  $\hat{u}$  of the Poincaré map.

Given the expansion of the return map for the scaled system (16), the locus of fixed points can be parameterized as a curve  $u = h(s; \mu, \eta)$ , as in (20) and (25). Let  $\hat{s} \in \mathbb{R}$  be such that  $\hat{u} = h(\hat{s}; 0, 0)$ , and  $z = s - \hat{s}$  evaluated from  $z = q(z; \mu, \eta)$ . Importantly, the right eigenvector  $v$  is tangent to the curve  $h$  at  $\hat{u} = h(\hat{s}; 0, 0)$ .

In blown-up coordinates, the limit cycle amplitude is  $\hat{\mathcal{A}} = \tilde{v}^- = \nabla H(y)^\top F(y)$ , and

$$\hat{\mathcal{A}} = C^\top A y + C^\top M + \mu C^\top A_1 y + \mu C^\top M_1 + o(\mu), \quad (45)$$

according to eq. (16). The amplitude in the coordinates of the original system is then simply given by  $\mathcal{A} = \hat{\mathcal{A}}\mu$ .

For small  $\mu > 0$  the fixed point is near  $\hat{u}$ , so we write  $u_p(\mu) = \hat{u} + \delta u$ . We have  $y = \zeta^{-1}(u_p) = \begin{bmatrix} 0 \\ u_p \end{bmatrix}$ , so

$$\delta u = z v + \text{H.O.T.} \quad (46)$$

Then from (45) we have

$$\hat{\mathcal{A}} = \ell_0 + \mu \ell_1 + L_{01} z + L_{11} \mu z + \text{H.O.T.} \quad (47)$$

where

$$\ell_0 = C^\top (A \zeta^{-1}(\hat{u}) + M), \quad \ell_1 = C^\top (A_1 \zeta^{-1}(\hat{u}) + M_1), \quad L_{01} = C^\top A \zeta^{-1}(v), \quad L_{11} = C^\top A_1 \zeta^{-1}(v).$$

To prove theorems 2 and 3 for the codimension-two saddle-node and period-doubling scenarios, we used Taylor expansions centred at  $(\mu, \eta) = (0, 0)$ . Now consider a nearby point  $(\mu, \eta) = (\mu_c, \eta_c)$  that belongs to the bifurcation curve of saddle-node or period-doubling bifurcations, and compute the limit cycle amplitude as a function of  $\mu$  with  $\eta = \eta_c$  fixed.

## B.1 The saddle-node case

To approximate the amplitude we truncate (20) to

$$q(z; \mu, \eta) = z + a\mu + b\eta + cz^2 + d\mu z + e\eta z + m\mu^2 + n\eta^2. \quad (48)$$

The fixed point equation for (48) is quadratic; by the quadratic formula the fixed points are

$$z = \mathcal{Y}_{1,2} - \frac{d\mu + e\eta}{2c}, \quad (49)$$

where

$$\mathcal{Y}_{1,2} = \pm \sqrt{\frac{(d\mu + e\eta)^2}{4c^2} - \frac{a\mu + b\eta}{c} - \frac{m\mu^2 + n\eta^2}{c}}.$$

Then by (47) if the blown-up system has two limit cycles for  $0 < \mu < \mu_c$ , these have amplitudes

$$\hat{\mathcal{A}} = \ell_0 + \mu\ell_1 + L_{01} \left( \pm \sqrt{-\frac{a}{c}(\mu - \mu_c) + \frac{(d^2 - 4mc)(\mu - \mu_c)^2}{4c^2}} - \frac{d(\mu - \mu_c)}{2c} \right), \quad (50)$$

where  $\ell_0 + \ell_1\mu_c$  is the amplitude of the fixed point  $\hat{u}$  at  $(\mu_c, \eta_c)$ , and  $L_{01}$  captures the variation in  $z$ . Multiplying this by  $\mu$  gives

$$\mathcal{A} = \ell_0\mu + \ell_1\mu^2 + \mu L_{01} \left( \pm \sqrt{-\frac{a}{c}(\mu - \mu_c) + \frac{(d^2 - 4mc)(\mu - \mu_c)^2}{4c^2}} - \frac{d(\mu - \mu_c)}{2c} \right). \quad (51)$$

## B.2 The period-doubling case

With a coordinate shift

$$\tilde{z} = z + \frac{a\mu + b\eta}{d\mu + e\eta - 2},$$

the map (25) can be written in the new coordinate as

$$\check{p}(\tilde{z}; \mu, \eta) = -\tilde{z} + \check{b}(\mu, \eta)\tilde{z} + \check{c}(\mu, \eta)\tilde{z}^2 + f\tilde{z}^3 + \text{H.O.T.},$$

where  $\check{c} = c - \frac{3f(a\mu + b\eta)}{d\mu + e\eta - 2}$ ,  $\check{b} = d\mu + e\eta - \frac{2c(a\mu + b\eta)}{d\mu + e\eta - 2}$ . We can transform the map into a normal form with a smooth coordinate transformation

$$\tilde{z} = y + \frac{\check{c}}{\lambda^2 - \lambda} y^2$$

where  $\lambda = -1 + \check{b}$ . We can now write

$$\check{p}(y) = \lambda y + \hat{c}y^3 + \mathcal{O}(y^4), \quad (52)$$

where  $\hat{c} = \frac{2\check{c}^2}{\lambda^2 - \lambda} + f$ . Further, after we apply the rescaling,

$$y = \frac{\gamma}{\sqrt{|\hat{c}|}},$$

the system takes the normal form with new coordinate

$$\tilde{\eta} = -(1 - \check{b})\gamma + \chi\gamma^3 + \mathcal{O}(\gamma^4),$$

where  $\chi = \text{sign}(\hat{c})$ . Near the period-doubling bifurcation, the period-two solution has points  $\gamma_{1,2} = \pm\sqrt{-\check{b}} + o((|\mu| + |\eta|)^{1/2})$  [28, pg, 125]. In  $z$ -coordinates the fixed point of the map is

$$\tilde{z} = h_1(\mu, \eta) = \frac{a\mu + b\eta}{2} + o(|\mu| + |\eta|)$$

while

$$\tilde{z}_{1,2} = \pm\sqrt{-\frac{\check{b}}{\hat{c}}} + \frac{\check{c}\check{b}}{|\hat{c}|(\lambda^2 - \lambda)} + h_1(\mu, \eta) + o(|\mu| + |\eta|) \quad (53)$$

are the points of the period-two solution.

Again, we treat  $\eta = \eta_c$  as fixed and assume the period-two solution exists for  $0 < \mu < \mu_c$ . Then the fixed point corresponds to a limit cycle with amplitude

$$\hat{\mathcal{A}} = \ell_0 + \ell_1\mu + L_{01}\frac{a(\mu - \mu_c)}{2} + o(|\mu| + |\mu - \mu_c|), \quad (54)$$

while the period-two solution corresponds to a limit cycle with amplitudes

$$\hat{\mathcal{A}} = \ell_0 + \ell_1\mu + L_{01}\left(\pm\sqrt{-\frac{(ca + d)(\mu - \mu_c)}{c^2 + f}} + \frac{c(ca + d)}{2(c^2 + f)}(\mu - \mu_c) + \frac{a(\mu - \mu_c)}{2}\right) + o(|\mu| + |\mu - \mu_c|). \quad (55)$$

Multiplying these by  $\mu$  gives the amplitudes in the original system coordinates.

## C Full equations of motion for the airfoil model

The model studied in [39, 40] is a reduced-order model of two-dimensional airfoil within a constant air stream. A full derivation can be found in [40]; here we simply specify the equations in full. The three mechanical degrees of freedom are  $\alpha$ ,  $\beta$ , and  $\zeta$ . The first two of these represent the angular displacement (pitch) of the airfoil and flap respectively, while  $\zeta = \frac{h}{b}$  is the dimensionless displacement in the heave degree of freedom, normalized by the semi-chord  $b$ . The parameter  $\bar{U} = \frac{U}{\omega_\alpha b}$  is a dimensionless measure of the magnitude of the free stream air velocity approaching the airfoil, and  $\delta$  characterizes the amount of flap freeplay.

Using Lagrangian mechanics one obtains the equations of motion of the mechanical degrees of freedom in the form

$$\bar{M} \begin{bmatrix} \ddot{\zeta} \\ \ddot{\alpha} \\ \ddot{\beta} \end{bmatrix} + \bar{C} \begin{bmatrix} \dot{\zeta} \\ \dot{\alpha} \\ \dot{\beta} \end{bmatrix} + \bar{K} \begin{bmatrix} \zeta \\ \alpha \\ \beta \end{bmatrix} = \begin{bmatrix} L/(mb) \\ T_\alpha/mb^2 \\ T_\beta/(mb^2) \end{bmatrix} + [\mathbf{F}] \quad (56)$$

$$\text{where } \bar{M} = \begin{bmatrix} 1 & \bar{x}_\alpha & \bar{x}_\beta \\ \bar{x}_\alpha & \bar{r}_\alpha^2 & \bar{r}_\beta^2 + \bar{x}_\beta(\bar{c} - \bar{a}) \\ \bar{x}_\beta & \bar{r}_\beta^2 + \bar{x}_\beta(\bar{c} - \bar{a}) & \bar{r}_\beta^2 \end{bmatrix},$$

$$\bar{K} = \begin{bmatrix} \omega_h^2 & 0 & 0 \\ 0 & \omega_\alpha^2 \bar{r}_\alpha^2 & 0 \\ 0 & 0 & \omega_\beta^2 \bar{r}_\beta^2 \end{bmatrix} \text{ and } \bar{C} = (\Phi^T)^{-1} \begin{bmatrix} 2\xi_h \omega_h & 0 & 0 \\ 0 & 2\xi_\alpha \omega_\alpha \bar{r}_\alpha^2 & 0 \\ 0 & 0 & 2\xi_\beta \omega_\beta \bar{r}_\beta^2 \end{bmatrix} \Phi^{-1},$$

where  $\Phi$  is an eigenvector matrix defined by  $(\bar{K} - \omega^2 \bar{M})\phi_i = 0$ ,  $\Phi = [\phi_1 \cdots \phi_n]$ , and  $\Phi^T \bar{M} \Phi = I$ . Also,  $L$ ,  $T_\alpha$ , and  $T_\beta$  define state-dependent generalised aerodynamic forces, defined below, and  $\mathbf{F}$  represents other external generalised forces (set to zero in the current model, except for preload  $1\% \cdot \delta k_\beta$  in the component corresponding to the rotational flap degree). Each  $\xi_i$ , for  $i \in \{h, \alpha, \beta\}$ , corresponds to the mode-proportional structural damping ratios for each degree of freedom; by default we set  $\xi_i = \xi = 0.02$  for each degree of freedom [43].

The unsteady aerodynamics  $L, T_\alpha, T_\beta$  are given as

$$\begin{aligned} L = \pi \rho_a b^2 & \left( \ddot{h} + V \dot{\alpha} - b \bar{a} \ddot{\alpha} - \frac{V}{\pi} T_4 \dot{\beta} - \frac{b}{\pi} T_1 \ddot{\beta} \right) \\ & + 2\pi \rho_a V b \left( Q_a(\hat{\tau}) \phi_w(0) - \int_0^{\hat{\tau}} Q_a(\sigma) \frac{d\phi_w(\hat{\tau} - \sigma)}{d\sigma} d\sigma \right), \end{aligned} \quad (57a)$$

$$\begin{aligned}
T_\alpha = & \pi\rho_a b^2 \left[ b\bar{a}\ddot{h} - Vb\left(\frac{1}{2} - \bar{a}\right)\dot{\alpha} - b^2\left(\frac{1}{8} + \bar{a}^2\right)\ddot{\alpha} - \frac{V^2}{\pi}(T_4 + T_{10})\beta \right. \\
& \left. + \frac{Vb}{\pi}\left(-T_1 + T_8 + (\bar{c} - \bar{a})T_4 - \frac{1}{2}T_{11}\right)\dot{\beta} + \frac{b^2}{\pi}(T_7 + (\bar{c} - \bar{a})T_1)\ddot{\beta} \right] \quad (57b)
\end{aligned}$$

$$\begin{aligned}
& + 2\pi\rho_a Vb^2\left(\bar{a} + \frac{1}{2}\right)\left(Q_a(\hat{\tau})\phi_w(0) - \int_0^{\hat{\tau}} Q_a(\sigma)\frac{d\phi_w(\hat{\tau} - \sigma)}{d\sigma}d\sigma\right), \\
T_\beta = & \pi\rho_a b^2 \left[ \frac{b}{\pi}T_1\ddot{h} + \frac{Vb}{\pi}\left(2T_9 + T_1 - \left(\bar{a} - \frac{1}{2}\right)T_4\right)\dot{\alpha} - \frac{2b^2}{\pi}T_{13}\ddot{\alpha} \right. \\
& \left. - \left(\frac{V}{\pi}\right)^2(T_5 - T_4T_{10})\beta + \frac{Vb}{2\pi^2}T_4T_{11}\dot{\beta} + \left(\frac{b}{\pi}\right)^2T_3\ddot{\beta} \right] \quad (57c) \\
& - \rho_a Vb^2T_{12}\left(Q_a(\hat{\tau})\phi_w(0) - \int_0^{\hat{\tau}} Q_a(\sigma)\frac{d\phi_w(\hat{\tau} - \sigma)}{d\sigma}d\sigma\right).
\end{aligned}$$

In order to approximate the unsteady aerodynamics, we use the exponential approximation to the Theodorsen functions

$$\phi(\tau) = 1 - a_1e^{-b_1\tau} - a_2e^{-b_2\tau},$$

as introduced by Jones [26]; see [43] for a derivation and definitions of the coefficients  $a_{1,2}$  and  $b_{1,2}$ . We then introduce the augmented variables

$$w_1(t) = \int_0^t Q_a e^{-b_1(t-\sigma)} d\sigma, \quad w_2(t) = \int_0^t Q_a e^{-b_2(t-\sigma)} d\sigma, \quad (58)$$

to calculate the aerodynamic forces  $L$ ,  $T_\alpha$ , and  $T_\beta$  in terms of feedback from the structural motion, where

$$Q_a = \left( V\alpha + \dot{h} + b\left(\frac{1}{2} - \bar{a}\right)\dot{\alpha} + \frac{V}{\pi}T_{10}\beta + \frac{b}{2\pi}T_{11}\dot{\beta} \right).$$

Then with  $X_s = [\zeta, \alpha, \beta]^\top$ , for the structural variables, and  $w_p = [w_1, w_2]^\top$  for the augmented parametric variables, the full coupled system is

$$\begin{aligned}
\dot{X}_s &= \dot{X}_s \\
M\ddot{X}_s &= -KX_s - C\dot{X}_s - D_w w_p \\
\dot{w}_p &= E_q X_s + E_{qd}\dot{X}_s + E_w w_p
\end{aligned} \quad (59)$$

where

$$M = \bar{M} - \eta M_{nc}, \quad K = \bar{K} - \eta(U/b)^2(K_{nc} + 0.5R_c S_{c1}), \quad C = \bar{C} - \eta(U/b)(B_{nc} + 0.5R_c S_{c2}),$$



$$D_\omega = \eta(U/b)R_c[a_1b_1(U/b)^2 \quad a_2b_2(U/b)], \quad E_q = (U/b)[S_{c1}; S_{c1}], \quad E_{qd} = [S_{c2}; S_{c2}],$$

$$E_\omega = \begin{bmatrix} -b_1 & 0 \\ 0 & -b_2 \end{bmatrix}, \quad \eta = 1/\pi\mu, \quad \text{and} \quad \mu = m/\pi\rho_a b^2,$$

$$M_{nc} = \begin{bmatrix} -\pi & \pi\bar{a} & T_1 \\ \pi\bar{a} & -\pi(1/8 + \bar{a}^2) & -2T_{13} \\ T_1 & -2T_{13} & T_3/\pi \end{bmatrix}, \quad B_{nc} = \begin{bmatrix} 0 & -\pi & T_4 \\ 0 & \pi(\bar{a} - 0.5) & -T_{16} \\ 0 & -T_{17} & -T_{19}/\pi \end{bmatrix}$$

$$R_c = \begin{bmatrix} -2\pi & \\ 2\pi(\bar{a} + 0.5) & \\ -T_{12} & \end{bmatrix}, \quad K_{nc} = \begin{bmatrix} 0 & 0 & 0 \\ 0 & 0 & -T_{15} \\ 0 & 0 & -T_{18}/\pi \end{bmatrix},$$

$$S_{c1} = \begin{bmatrix} 0 & 1 & \frac{T_{10}}{\pi} \end{bmatrix}, \quad S_{c2} = \begin{bmatrix} 1 & 0.5 - \bar{a} & \frac{T_{11}}{2\pi} \end{bmatrix},$$

with all  $T_i$  constants given in [41].

Finally we transform the differential-integral equations eq. (56) into the following system of first-order ODEs:

$$\begin{bmatrix} \dot{X}_s \\ \ddot{X}_s \\ \dot{w}_p \end{bmatrix} = \begin{bmatrix} 0_{3 \times 3} & I_{3 \times 3} & 0_{3 \times 2} \\ -M^{-1}K & -M^{-1}C & -M^{-1}D \\ E_q & E_{qd} & E_w \end{bmatrix} \begin{bmatrix} X_s \\ \dot{X}_s \\ w_p \end{bmatrix} + \begin{bmatrix} 0_{3 \times 1} \\ -M^{-1}F(X_s) \\ 0_{2 \times 1} \end{bmatrix}. \quad (60)$$

The physical parameters used in this study are given in appendix C.

Table 1: Parameter Definition

Physical parameters					
$b$	$\omega_h$	$\omega_\alpha$	$\omega_\beta$	$\rho_a$	$m$
0.3 m	50 rad/s	100 rad/s	0 rad/s	1.225 kg/mm <sup>3</sup>	1.5 kg
$a_1$	$a_2$	$b_1$	$b_2$	$\xi_i, i = h, \alpha, \beta$	$r$
0.165	0.0455	0.335	0.3	2%	0.72
Dimensionless parameters					
$\bar{a}$	$\bar{c}$	$\bar{x}_\alpha$	$\bar{x}_\beta$	$\bar{r}_\alpha^2$	$\bar{r}_\beta^2$
-0.4	0.6	0.2	0.0125	0.25	0.00625

For convenience, we also specify here the numerically evaluated matrices needed to compute the normal form eq. (6). At the BEB  $\bar{U} = 0.64833$  and  $\delta = 0.01$  rad, we obtained

$$\mathbf{A} = [\mathbf{A}_1 \quad \mathbf{A}_2]$$

where

$$\mathbf{A}_1 = \begin{pmatrix} 0 & 0 & 0 \\ 0 & 0 & 0 \\ 0 & 0 & 0 \\ -2.9340e+03 & 2.3800e+03 & -31.8848 \\ 2.5143e+03 & -1.4569e+04 & -126.9591 \\ -1.5787e+03 & 3.9373e+04 & 119.8092 \\ 0 & 0 & 0 \\ 0 & 64.8330 & 35.6462 \end{pmatrix},$$

$$\mathbf{A}_2 = \begin{pmatrix} 1 & 0 & 0 & 0 & 0 \\ 0 & 1 & 0 & 0 & 0 \\ 0 & 0 & 1 & 0 & 0 \\ -4.1409 & -1.7578 & -0.2147 & -118.8655 & -29.0256 \\ 3.3583 & -8.2454 & -1.0773 & 157.7863 & 38.5297 \\ -3.2826 & 17.0083 & -1.9570 & -328.2203 & -80.1478 \\ 0 & 0 & 0 & 0 & 1 \\ 1 & 0.9000 & 0.1487 & -57.3753 & -22.3998 \end{pmatrix},$$

and, regarding the reset map,

$$\mathbf{C} = \begin{pmatrix} 0 \\ 0 \\ 1 \\ 0 \\ 0 \\ 0 \\ 0 \\ 0 \\ 0 \end{pmatrix}, \quad \mathbf{B} = (1+r) \begin{pmatrix} 0 \\ 0 \\ 0 \\ 0.0030 \\ -0.0774 \\ 1 \\ 0 \\ 0 \end{pmatrix}.$$